AFRL-PR-WP-TR-2006-2203

HEAT TRANSFER ENHANCEMENT THROUGH SELF-SUSTAINED OSCILLATING FLOW IN MICROCHANNELS

C.X. Lin, Ph.D.

Florida International University
Applied Research Center
10555 West Flagler Street, EC 2100
Miami, FL 33174

MAY 2006

Final Report for 17 October 2003 – 17 May 2006

PROPULSION DIRECTORATE
AIR FORCE MATERIEL COMMAND
AIR FORCE RESEARCH LABORATORY
WRIGHT-PATTERSON AIR FORCE BASE, OH 45433-7251

NOTICE AND SIGNATURE PAGE

Using Government drawings, specifications, or other data included in this document for any purpose other than Government procurement does not in any way obligate the U.S. Government. The fact that the Government formulated or supplied the drawings, specifications, or other data does not license the holder or any other person or corporation; or convey any rights or permission to manufacture, use, or sell any patented invention that may relate to them.

This report was cleared for public release by the Air Force Research Laboratory Wright Site (AFRL/WS) Public Affairs Office and is available to the general public, including foreign nationals. Copies may be obtained from the Defense Technical Information Center (DTIC) (http://www.dtic.mil).

AFRL-PR-WP-TR-2006-2203 HAS BEEN REVIEWED AND IS APPROVED FOR PUBLICATION IN ACCORDANCE WITH ASSIGNED DISTRIBUTION STATEMENT.

*//Signature//

TRAVIS E. MICHALAK
Technical Monitor
Power Division

//Signature//

JOHN G. NAIRUS
Chief, Electrochemistry and Thermal Sciences Branch
Power Division

//Signature//

KIRK L. YERKES
Deputy for Science
Power Division

This report is published in the interest of scientific and technical information exchange, and its publication does not constitute the Government's approval or disapproval of its ideas or findings.

*Disseminated copies will show "//Signature//" stamped or typed above the signature blocks.

REPORT DOCUMENTATION PAGE

Form Approved
OMB No. 0704-0188

1. REPORT DATE *(DD-MM-YY)*	2. REPORT TYPE	3. DATES COVERED *(From - To)*
May 2006	Final	10/17/2003 – 05/17/2006

4. TITLE AND SUBTITLE
HEAT TRANSFER ENHANCEMENT THROUGH SELF-SUSTAINED OSCILLATING FLOW IN MICROCHANNELS

5a. CONTRACT NUMBER
FA8650-04-C-2405

5b. GRANT NUMBER
MDA HBCU/MI BAA 2003-01

5c. PROGRAM ELEMENT NUMBER
63175C

6. AUTHOR(S)
C.X. Lin, Ph.D.

5d. PROJECT NUMBER
1602

5e. TASK NUMBER
FU

5f. WORK UNIT NUMBER
00

7. PERFORMING ORGANIZATION NAME(S) AND ADDRESS(ES)
Florida International University
Applied Research Center
10555 West Flagler Street, EC 2100
Miami, FL 33174

8. PERFORMING ORGANIZATION REPORT NUMBER

9. SPONSORING/MONITORING AGENCY NAME(S) AND ADDRESS(ES)
Propulsion Directorate
Air Force Research Laboratory
Air Force Materiel Command
Wright-Patterson AFB, OH 45433-7251

10. SPONSORING/MONITORING AGENCY ACRONYM(S)
AFRL-PR-WP

11. SPONSORING/MONITORING AGENCY REPORT NUMBER(S)
AFRL-PR-WP-TR-2006-2203

12. DISTRIBUTION/AVAILABILITY STATEMENT
Approved for public release; distribution is unlimited.

13. SUPPLEMENTARY NOTES
PAO case number: AFRL/WS 06-2021; Date cleared: 21 Aug 2006. This report contains color.

14. ABSTRACT

This is the final report on contract FA8650-04-C-2405, an MDA grant (MDA HBCU/MI BAA 2003-01) to Florida International University. The main objectives of this research were to understand the hydraulic and thermal characteristics of self-sustained oscillating flow through microchannels, and then to obtain correlations of parameters to assist in the design of heat sinks / heat exchangers that would utilize this oscillating flow to improve the thermal management of electronics. The oscillating flows are achieved by placing vortex generating blocks in the microchannels to create the oscillating vortices that are meant to enhance heat transfer. Experimental studies were carried out on various configurations of microchannels, with various numbers of vortex generators, and the results were reported. Also, the results of a numerical study on the heat transfer and hydraulic behavior around the vortex generators are reported.

15. SUBJECT TERMS
heat transfer, electronics cooling, self-sustained, oscillating flow, microchannel flow, vortex generators, MDA grant report

16. SECURITY CLASSIFICATION OF:			17. LIMITATION OF ABSTRACT:	18. NUMBER OF PAGES	19a. NAME OF RESPONSIBLE PERSON (Monitor)
a. REPORT	b. ABSTRACT	c. THIS PAGE			Travis E. Michalak
Unclassified	Unclassified	Unclassified	SAR	58	19b. TELEPHONE NUMBER *(Include Area Code)* N/A

TABLE OF CONTENTS

1 INTRODUCTION

1.1. Research Background

Heat generated by electronic devices, laser arrays, and power sources in Missile Defense Agency (MDA) facilities needs to be dissipated effectively to ensure that temperature-sensitive components function properly and achieve their maximum performance. However, the thermal management needs at MDA are often more challenging than those in industry because of weight and volume limitations in the platforms. To remove heat dissipation at the rate above 10^6 W/m^2, the heat transfer requirement is beyond the capabilities of the conventional cooling methods. Microchannel (1 μm < hydraulic diameter < 1 mm) heat sink, introduced by Tuckerman and Pease[1] in the early 1980s, is an innovative cooling technology, which could achieve very high rate of energy flow by forcing the cooling fluid through microchannels fabricated directly in the silicon wafer containing heat-dissipating large scale integrated circuit (LSIC) components. This new technology demonstrates two advantages over the conventional heat transfer methods. The first one is that microchannel can be manufactured near where the heat source is located without impacting the mechanical structure and therefore is capable of catching heat where it is generated. The shorter heat conduction path between the heat source and the sink in this microchannel heat sink configuration results in a much lower thermal resistance. The other advantage of the microchannel heat sink is its superior cooling capacity due to the great surface area per unit volume of microchannels.

Even though microchannel heat sinks are capable of dissipating much higher heat fluxes than conventional cooling techniques, two existing problems are limiting their applications. The first one is the large pressure drop along the flow direction caused by the microscale hydraulic diameter, which requires more pumping power. The second problem is that the low flow rate in microchannel produces large temperature rise along the flow direction in both the cooling fluid and the solid walls, which may damage temperature-sensitive electronic components of LSIC. The problem becomes worse if temperature

distribution on a plate or a printed circuit board is highly biased.

To fully utilize the advantages of microchannel cooling technology, such as high energy mitigation capability and low heat resistance and effectively solve the existing two problems encountered by plane microchannels, i.e., high pressure drop and high channel-wise temperature rise, this research project is going to apply vortex generator (VG) technology[2-4] in microchannels, i.e., periodically mounting arrays of square cylinders/bars in microchannel to generate self-sustained oscillating flow. Since the ordered laminar oscillating flow requires much less pumping power than turbulent flow to achieve the same heat transfer rate or to get a much higher heat transfer rate at the same pumping power, due to the advantage of ordered laminar self-sustained oscillation over random turbulent fluctuations which yields less viscous dissipation. Meanwhile, the strong convective mixing among the communicating channels helps reducing the channel-wise temperature rise. A numerical simulation was reported that this VG equipped microchannel yields much higher cooling capacity than plane microchannels without causing a large pressure drop[5]. This new technology is being anticipated to be used in MDA applications to design more efficient and more reliable microchannel heat sinks or microchannel heat exchangers with high heat dissipation capabilities ($>10^6$ W/m^2) and low heat resistance in order to meet the increasing heat dissipation demand for MDA electronic devices at ground, air, and space platforms at both ambient/room and cryogenic temperatures.

To the best of the investigators' knowledge, currently there are no available experimental data in the open literature that could lead to a practical design for self-sustained oscillating flow in microchannels. Furthermore, traditional numerical approaches, such as those using Navier-Stokes equations, are not able to correctly predict the hydraulic and thermal behaviors of microchannel flows. The experimental results have shown that fluid flow and heat transfer characteristics of microchannels deviate from that of conventionally sized channels (macroscale, hydraulic diameter > 1 mm)[6-9]. For liquid flow in microchannels, the flow characteristics are more complicated than that of gas. In addition to the rarefaction effect, effects of electric double layer (EDL)[10] and dissolved noncondensable vapor[11] could

account for a certain percentage (about the order of 10%) of the heat transfer rate variations in microchannel flows, which were usually negligible in macroscale channel flows. To date, there have been no acceptable models for simulating liquid flow in microchannels that take into accounts all of the effects due to the microscale size.

The available investigations on the physical mechanism of heat transfer enhancement by oscillating flow was primarily concentrated on VG equipped conventionally sized channels through both experimental and numerical methods [12-23]. It was found that the heat transfer rate and pressure drop are both increasing. The physical mechanism of heat transfer enhancement for VG equipped conventionally sized channels was concluded as follows [20]:

- Surface interruption prevents the continuous growth of the thermal boundary layer by periodically interrupting it. This mechanism occurs even at low Reynolds numbers when the flow is steady and laminar;
- Above a critical Reynolds number, the interrupted surfaces offer an additional mechanism of heat transfer enhancement by inducing oscillations in the flow in the form of shed vortices. These vortices enhance local heat transfer by continuously bringing fresh fluid towards the heat transfer surfaces;
- In addition to heat transfer enhancement, surface interruption increases the friction loss and thus requires larger pumping power. This is partly due to the larger skin friction associated with the hydrodynamic boundary layer restarting. In the unsteady flow regime, the time-dependent flow behavior associated with vortex shedding increases friction loss through the stokes layer dissipation and form drag through Reynolds stresses;
- The boundary layer restart and self-sustained oscillatory mechanisms simultaneously influence both the overall heat transfer and the pumping power requirement.

While for the investigation on VG equipped microchannel flows, only one numerical study is available[5]. The numerical results indicated that this VG equipped microchannel yields much higher heat transfer rate without causing a large pressure drop, which is different from that of conventionally sized channels. This numerical observation greatly encourages this project to investigate the physical mechanism of heat transfer performance and flow resistance on VG equipped microchannel flows.

In this project, a series of experimental studies, including micro-particle image velocimetry (PIV), hydraulic and thermal measurements will be carried out to reveal the physical mechanism of self-sustained oscillating flow on heat transfer and flow resistance in microchannels. In addition, comprehensive parameter studies will be conducted to obtain correlations among the critical control parameters, such as the Reynolds number, Nusselt number and channel geometric parameters, which will become unique criteria for the future design of microchannel heat sinks.

1.2. Project Objectives

Self-sustained oscillating flow in microchannels is a promising new concept in thermal management. Once it is well understood, it can be used for the cooling of electronic devices or other equipment that requires large heat transfer flux concerned with high temperature sensitive components in MDA related systems. The primary objectives of this project are:

- To understand the hydraulic and thermal characteristics of self-sustained oscillating flow through microchannels. Flow visualization, flow spectrum study, and pressure drop and temperature measurements will be conducted for single-row and multi-row channels to investigate the physical mechanisms of flow and heat transfer. For the single-row channel, the focus will be the characteristics of heat transfer and pressure drop. For the multi-row channel, the fluid mixing processes among communicating channels will be the research focus in addition to the heat transfer and flow resistance characteristics.

- To obtain correlations and recommend parameters for the optimum design of a highly efficient heat sink or heat exchanger. Various parameters, such as streamwise and transverse-wise pitches, block ratio, Reynolds number (and/or Prandtl number) will be varied to investigate their influence on the target parameters, such as the Nusselt number and the apparent friction coefficient. The generated database will become a unique reference for the development or design of a highly efficient heat sink or heat exchanger.

1.3. Significance of the Project

This project will contribute to the MDA's Innovative Science and Technology Program goal of establishing advanced thermal management approaches to enable electronic devices to achieve their maximum performance with reduced pumping power and temperature sensitivity, and meanwhile greatly enhance Florida International University (FIU)'s research and development capabilities related to the needs of MDA, which will lead to FIU's future participation in the primary MDA research programs.

With an enrollment of over 33,000 students, including about 70% minority students, FIU is the largest producer of Hispanic engineering graduates in the nation. It provides a good chance to expose minority students to new technology development in the field of thermal management.

2 Experimental Study

2.1 Experimental setup

Figure 1 shows the picture of the hydraulic loop used for the experimental investigations of this project. Schematic diagram of the loop is shown in Figure 2 for the convenience of recognizing each component. In the experimental study, DI water was pumped through a 5-μm filter to prevent any particles from entering the microchannels and creating blockages. A micro flow meter was installed downstream of the filter to measure the flow rate, local temperature and hydraulic loop pressure of the flowing water. Before entering the test section, the DI water was directed into a temperature controlled water bath to keep the inlet water temperature at a constant value in the range of 20-100^{0}C for each run of test. The water temperature was increased after flowing through the heated test section and than cooled down to a certain value around the inlet temperature through a chill water heat exchanger located downstream of the test section exit. After leaving the heat exchanger, the DI water returned to the pump, completing the hydraulic loop.

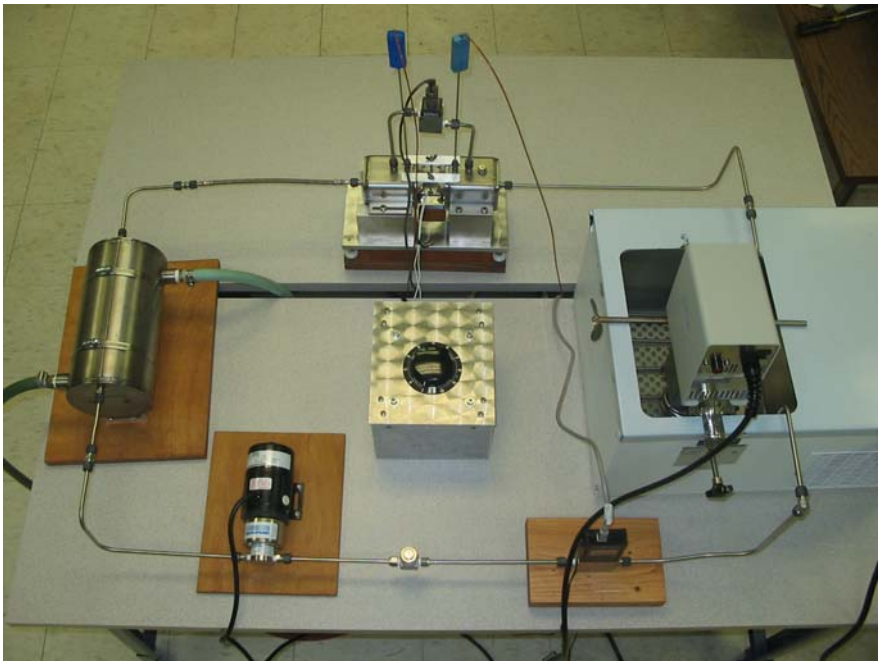

Fig. 1 Photograph of the hydraulic loop.

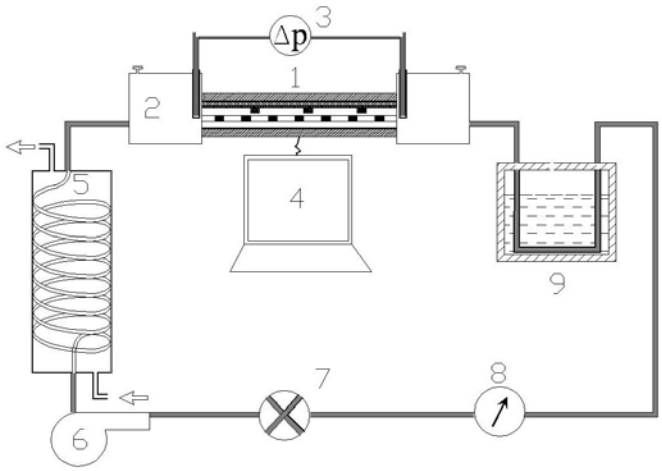

1	Test Section
2	Plenum
3	Differential Pressure Transducer
4	Data Acquisition System
5	Heat Exchanger
6	Gear Pump
7	Filter
8	Flow Meter
9	Water Bath

Fig. 2 Schematic diagram of the hydraulic loop.

Test section

Each test section was composed of three plates/chips: the capping/bottom plate was made of quartz for visualization study, and the middle and top plates were made of silicon wafer. VG cube arrays were fabricated in the middle one and the top plate was used for mechanical support and thermal couple installations.

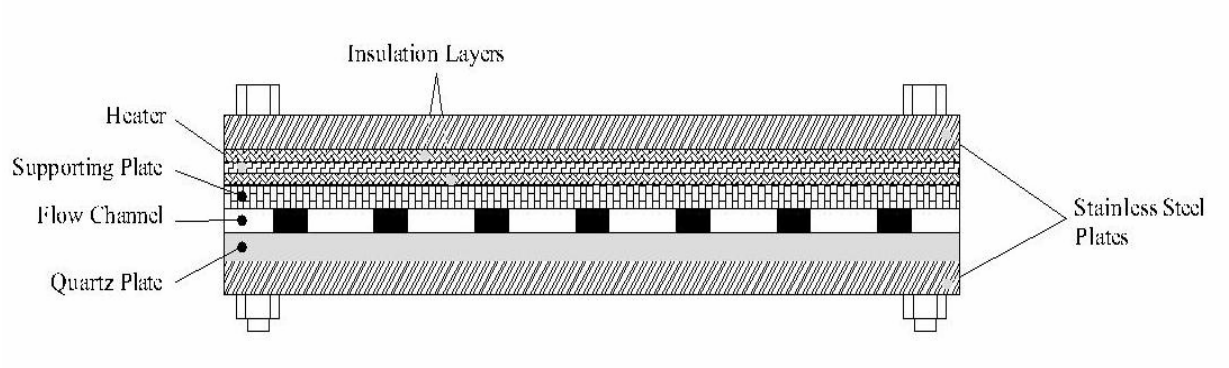

Fig. 3 Cross-section view of the test section.

The three chips were bonded together with epoxy resin to form a flow channel (Figure 3) and connected with two plenums for the convenience of temperature and pressure drop measurements (Figure 4). Two thermocouples were inserted into the plenums to measure the inlet and outlet temperatures, respectively. The test section pressure drop was measured by the pressure transducer. Five pairs of thermocouples were embedded in five measurement slots fabricated in the supporting plate to measure the surface temperature of the flow channel. The empty of the slots was filled with aluminum nitride powder to maintain constant thermal boundary conditions. The thermocouples were covered by an electrical insulating layer to prevent any electrical interference with the heater. The heat input was delivered through an electrical heater (0-1200 W) attached to the supporting plate, and adjusted through a variable transformer. The test section and heater were well insulated to minimize the heat loss to the surroundings, and sandwiched with stainless steel plates for the safe assembling with the plenums.

Connection with plenums

Close up of the test section and plenum connection is shown in Figure 4. The assembled test section was first glued horizontally to two connecting plates by inserting the test section into the slots fabricated in each plate. The ending of the slots was made exactly identical to the height and width of the test section and the opening was cut slightly larger, for the purpose of preventing any overflow of the glue through the slots into the micro-sized flow channels. The two connecting plates were fastened tightly to the plenums with plastic gaskets to make the connection watertight. The sandwiched test section was rigidly supported with stainless steel plates and bolts to avoid any stresses or loads applied on the microchannel chips.

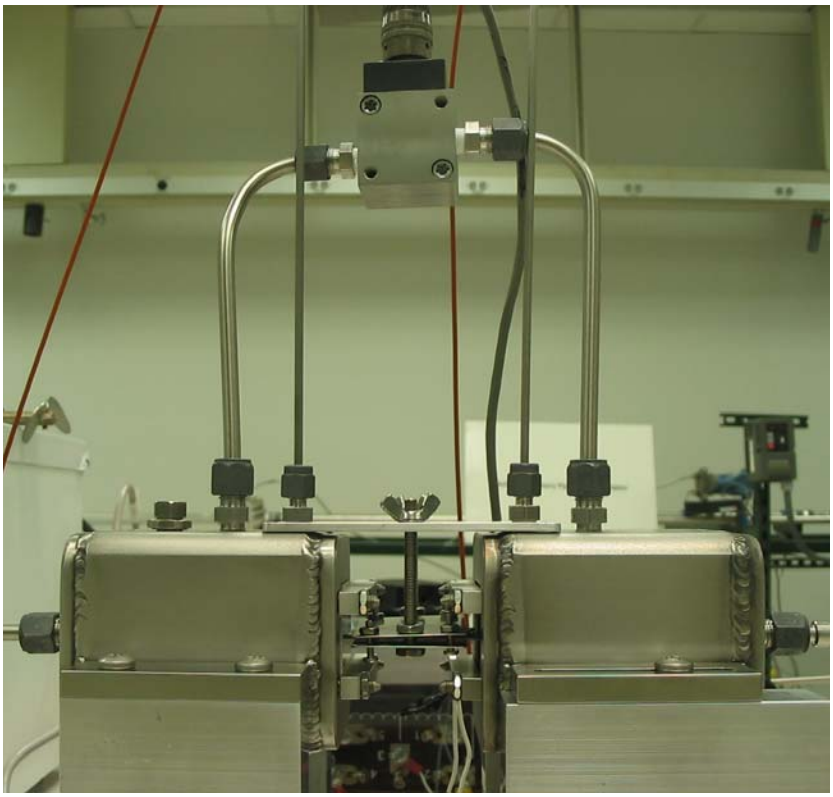

Fig. 4 Test section and plenum connection.

Verification of Instrumentation Calibration

After the loop was checked for leakage, calibration of individual devices and components was tested against the calibration results provided by the vendors.

Differential pressure transducer was tested by measuring the pressure drop in a straight tube (33" long) oriented horizontally and comparing measurements with the calculated results from the Darcy- Weisbach equation:

$$\Delta P = f \frac{L}{D_h}\left[\frac{1}{2}\rho V^2\right] \quad (1)$$

Where f is friction factor and D_h is the hydraulic diameter.

The comparison results are shown in Figure 5. It can be seen that the pressure transducer readings are larger than the theoretical values at large flow rates, which could be due to the tube flow being not fully developed in the whole measurement length, while the friction factor is smaller for fully developed flow which is assumed in the theoretical calculations. The differential pressure transducer is calibrated by the vendor to an accuracy of ±0.25 % of the full measurement range (Figure 6), which is not repeatable or attainable with the present experimental devices and is assumed to be acceptable.

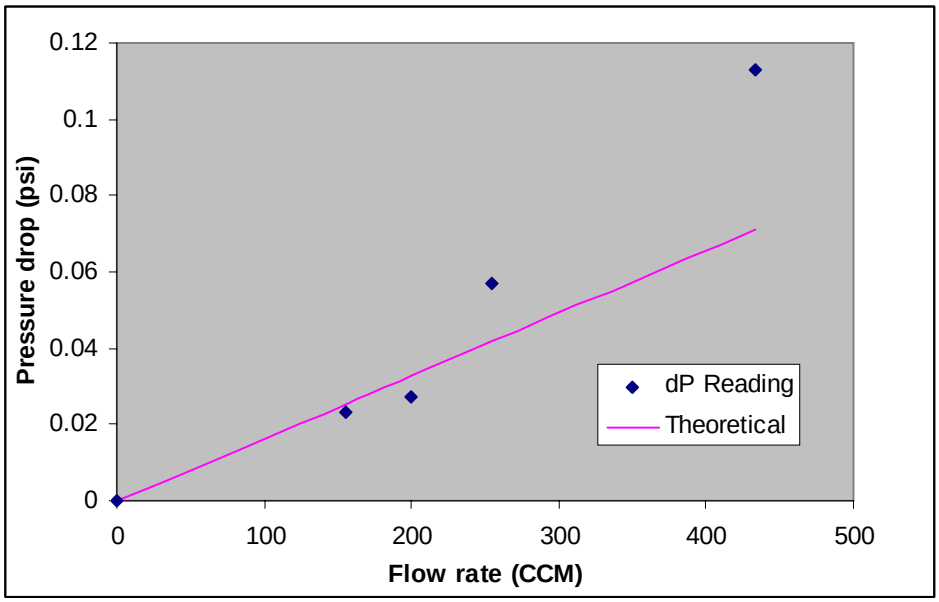

Figure 5. Pressure drop comparison

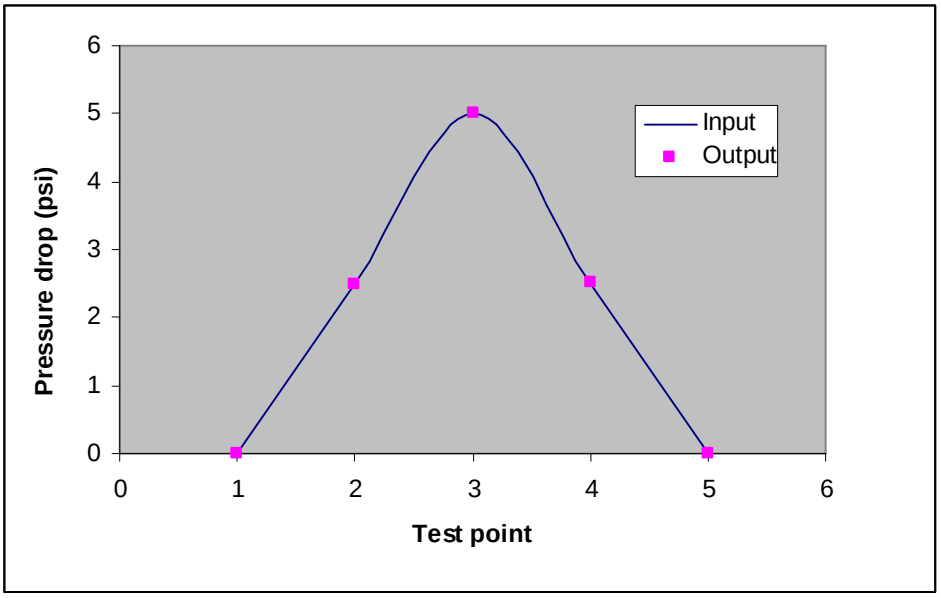

Figure 6. Vendor provided calibration results for the differential pressure transducer.

The flow meter was tested by measuring the volume of water with a measuring jar and the time with a stop watch. The measured results are compared with the flow meter readings in Figure 7. The deviation of the readings is up to 22% of the measured value at low flow rate, and within ±5% at larger one. This result is close to the accuracy of ± 2% provided by the vendor.

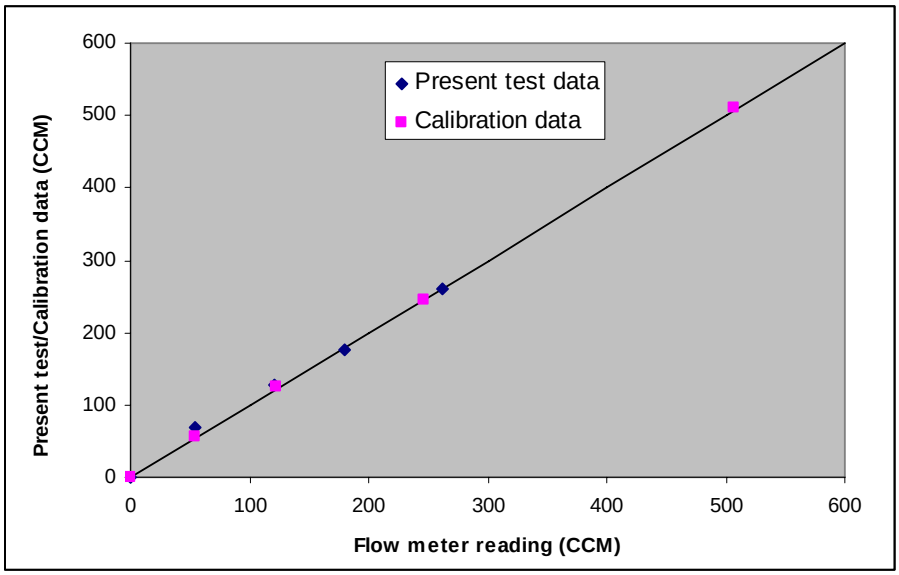

Figure 7. Flow meter tests

All thermocouples have been tested at two different temperatures, 0 ^{0}C, provided by ice-water mixture and 100 ^{0}C, provided by boiling water, at atmospheric pressure (Figure 8). The accuracy is within ±0.2 ^{0}C, which is the calibration accuracy provided by the vendor.

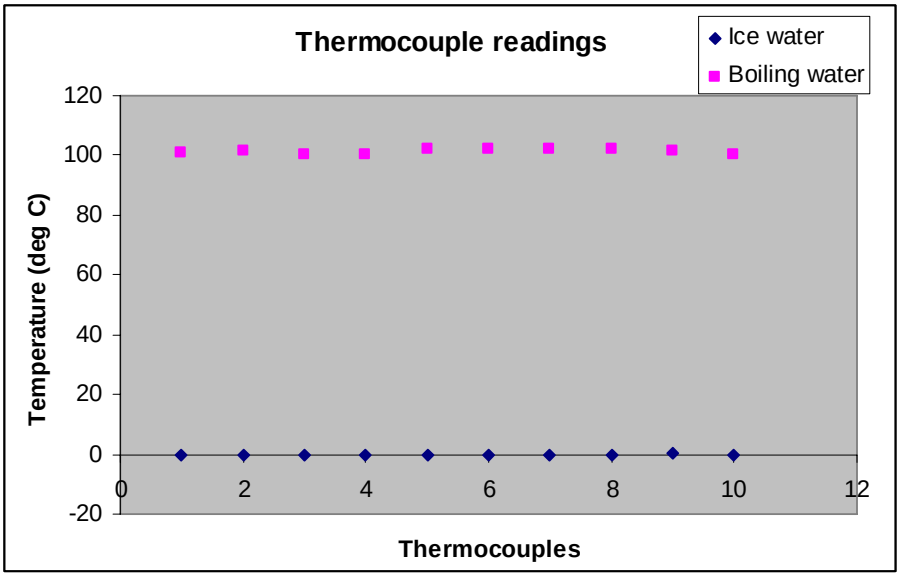

Figure 7. Thermocouple calibrations

2.2 Data collection and reduction

A LabVIEW data acquisition system was used for data collection. After the loop has been running for a certain period of time, steady state was assumed when the temperature variation was less than ±1% within 5 minutes. All temperature, flow rate and pressure drop data were then recorded.

The hydraulic diameter, d_h of the test section is defined as:

$$d_h = \frac{4A_c}{P} \tag{2}$$

Where A_c is the cross-section area of the microchannel and P is the perimeter.

The Reynolds number, Re is given by:

$$Re = \frac{\rho u d_h}{\mu} \tag{3}$$

Where u is the mean velocity of water; μ is the dynamic viscosity and ρ is the density. The reference temperature for properties is taken as the average of the wall temperatures and the fluid inlet and outlet temperatures.

The Nusselt number, *Nu* is given as:

$$Nu = \frac{hd_h}{k} \tag{4}$$

Where h is the heat transfer coefficient of water and k is the thermal conductivity.

The friction factor, f is calculated from the pressure drop across the micro channel:

$$f = \frac{2\Delta P d_h}{L\rho u^2} \tag{5}$$

Where L is the microchannel length and ΔP is the pressure drop.

2.3 Experimental results and discussions

Upon successful testing and calibration of the hydraulic flow loop heat transfer studies with the VG-equipped microchannels were conducted.

Figures 8 and 9 present the variations of *Nu* and f with respect to *Re* for the VG-equipped microchannel with one row of 40 VG cubes. Other dimensions of this microchannel are as follows: height 505 μm, length 39895 μm, and width 2525 μm. Experimental results are compared on the same figures with the correlations developed for smooth microchannels [31]:

$$Nu_{lam} = 0.1165\left(\frac{d_h}{W_c}\right)^{0.81}\left(\frac{H}{W}\right)^{-0.79} Re^{0.62}\, Pr^{1/3} \tag{6}$$

$$Nu_{turb} = 0.072\left(\frac{d_h}{W_c}\right)^{1.15}[1-2.421(Z-0.5)^2]\, Re^{0.8}\, Pr^{1/3} \tag{7}$$

$$f_{lam} = \frac{C_{f,lam}}{Re^{1.98}} \tag{8}$$

$$f_{turb} = \frac{C_{f,turb}}{Re^{1.72}} \tag{9}$$

Where *Pr* is the Prandtl number; W_c is the microchannel center to center spacing; Z is the dimensionless parameter [31]; C_f is the empirical coefficient. Subscripts *lam* stands for laminar and *turb* for turbulent.

From Figures 8 and 9, it can be observed that with one row of VG cubes mounted in the microchannels, *Nu* is larger than that predicted by laminar correlation and smaller that predicted by turbulent one at *Re*<630, where the flow regime is not determined in the present study. The *f* is larger than the laminar correlation predictions at *Re* > 400, and also larger than the turbulent correlation predictions at *Re* > 670.

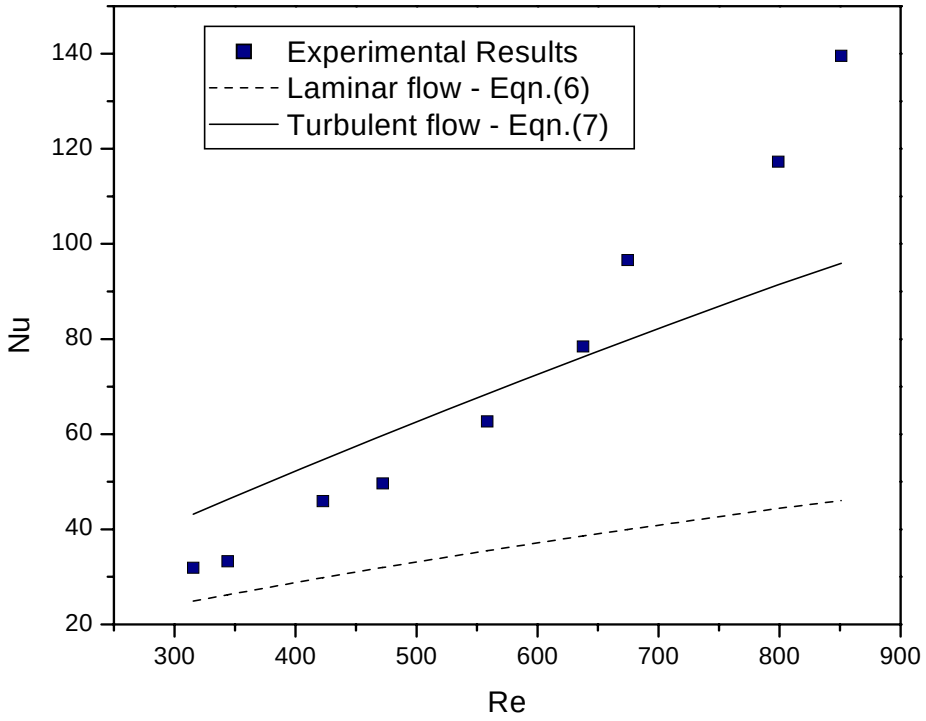

Figure 8. *Nu* vs. *Re* for the 1x40 cube array microchannel.

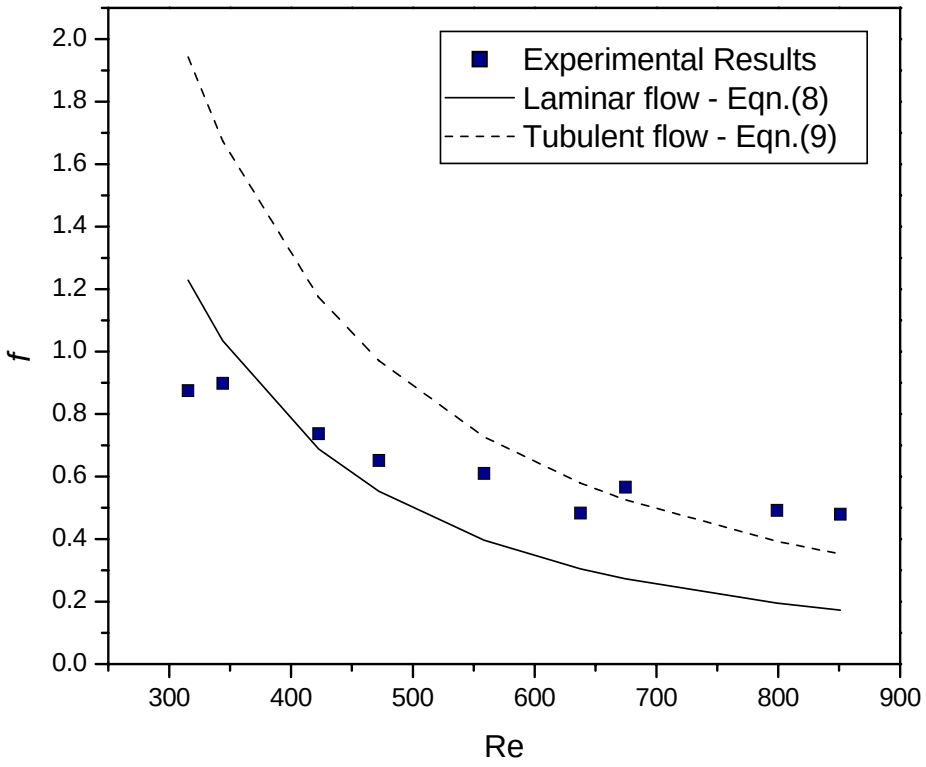

Figure 9. *f* vs. *Re* for the 1x40 cube array microchannel.

As shown in Figure 10, *fRe* is much larger and oscillating with *Re*. The temperature ratio, shown in Figure 11, shows that the temperature increases more in the water flow direction than that on the wall, indicating the improvement of wall temperature distribution by VG cubes.

These experimental results indicate that VG cubes could improve the heat transfer and wall temperature distribution in microchannel compared with smooth one, while the flow resistance is larger.

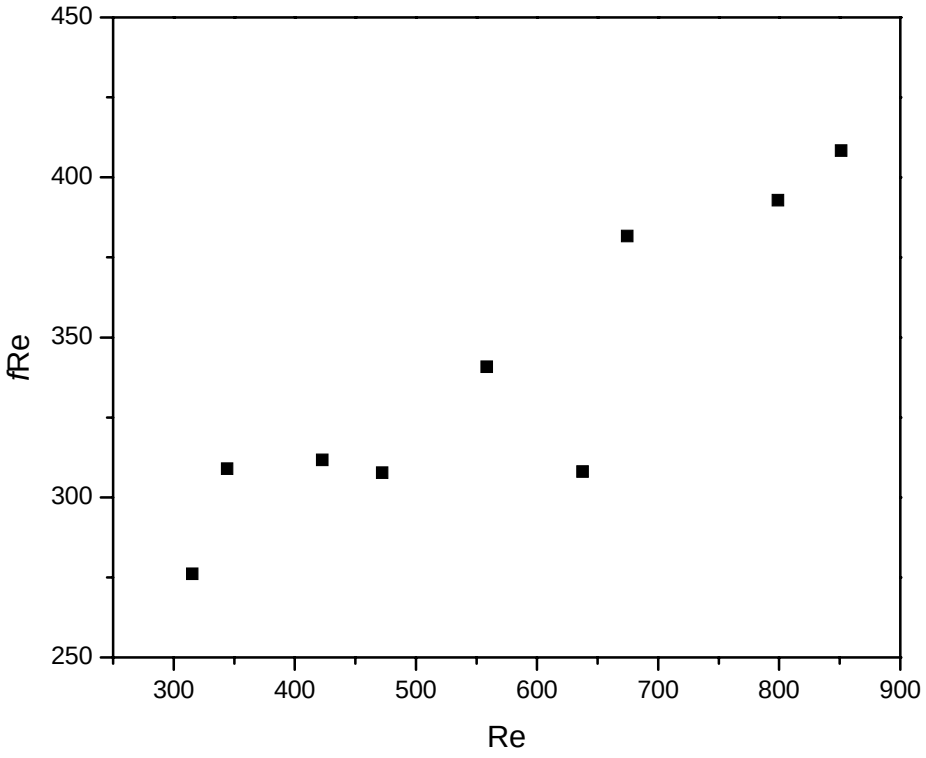

Figure 10. *fRe* vs. *Re* for the 1x40 cube array microchannel.

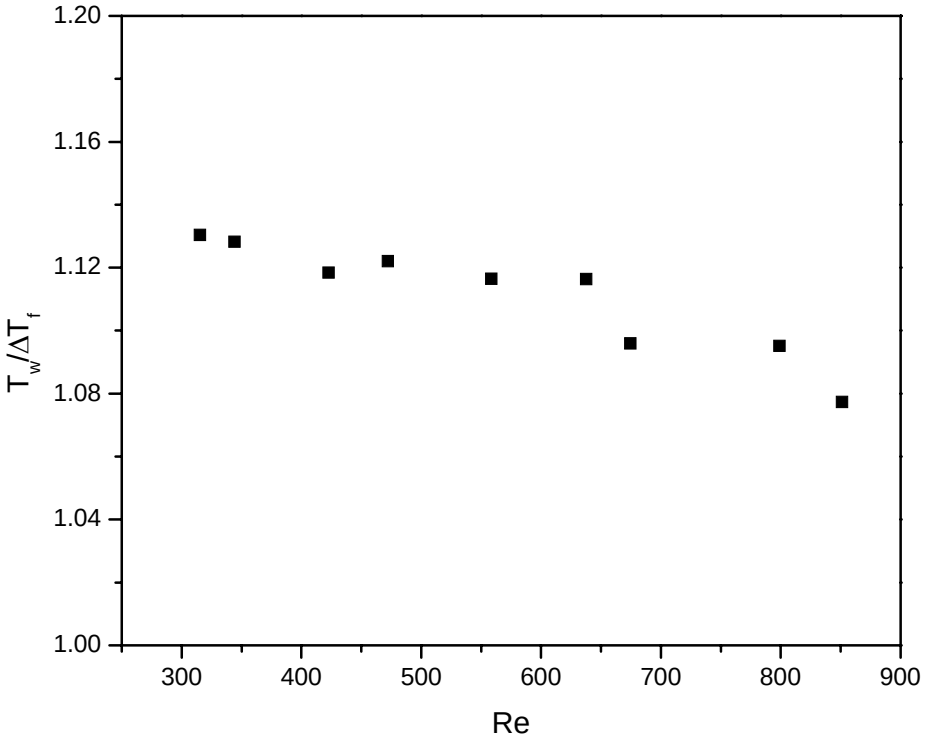

Figure 11. Temperature ratio vs. *Re* for the 1x40 cube array microchannel.

The effects of the inlet fluid temperature and the heat input have been studied for a multi-row VG-equipped microchannel. This channel has 7 × 21 array of VG cubes, its other dimensions are as follows: height 505 µm, length 39895 µm, and width 11615 µm. Three different inlet fluid temperatures have been tested for two different heat inputs. Figure 12 presents the variations of Nu with respect to Re. As can be seen from the graphs, with the increase of inlet fluid temperature the Nusselt number is increased for the given test conditions. It should be noted that with the increase of Reynolds number, the Nusselt number doesn't vary much. It can also be noted that the Nusselt number is almost the same for the different heat input conditions with the same inlet fluid temperature. This could further prove that the Nusselt number doesn't change much with change in heat flux.

For a fixed Re = 200, the effects of change in inlet fluid temperature on the Nusselt number is given in Figure 13. There was an average increase of 40 % in the Nusselt number when the temperature of the inlet fluid has been increased by 5 ^{o}C.

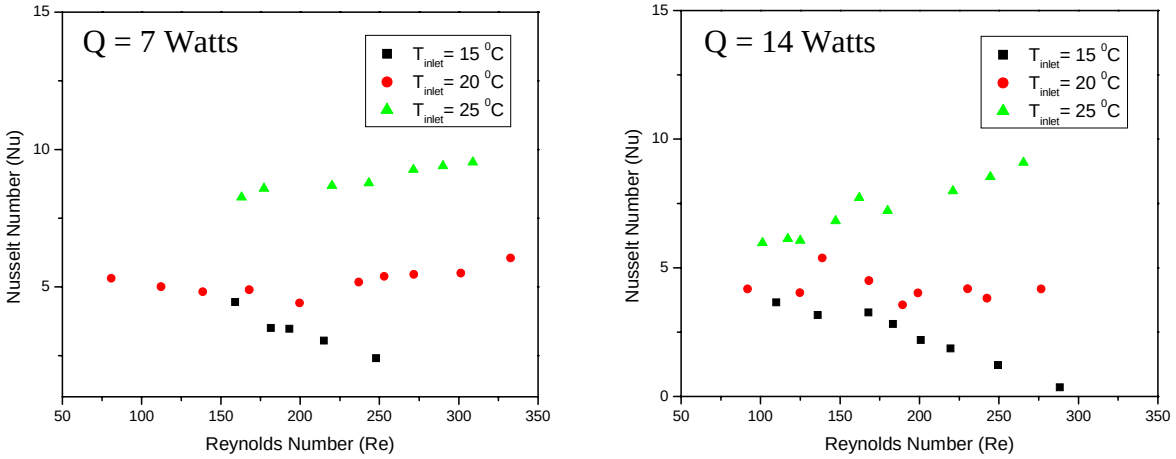

Figure 12. Nu vs. Re for the 7 × 21 cube array microchannel.

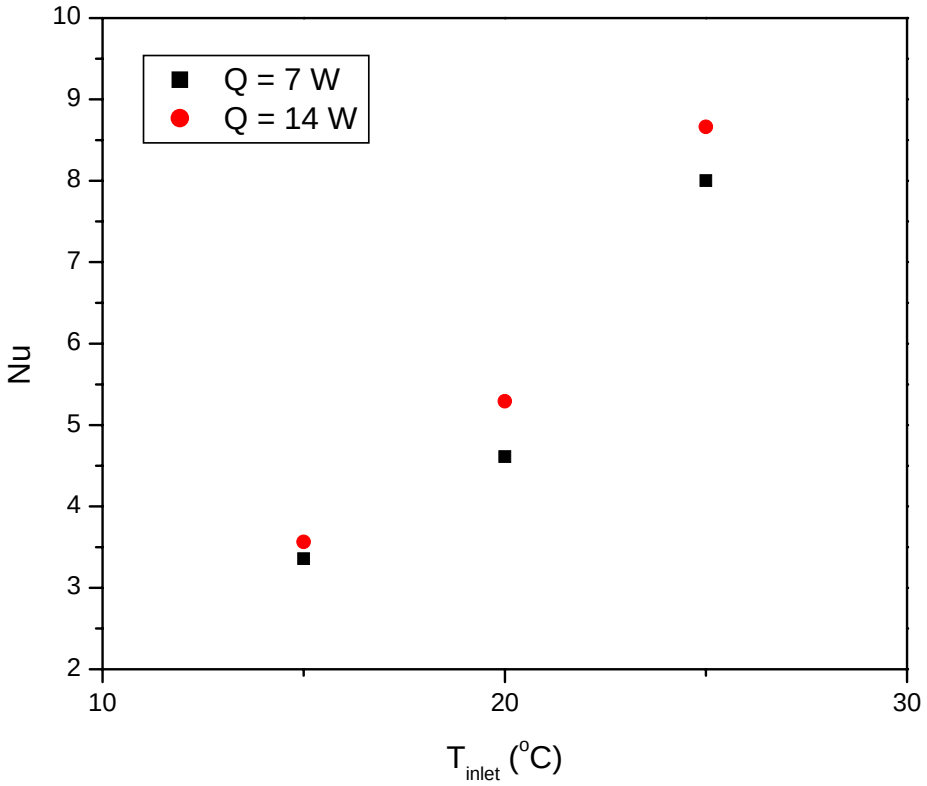

Figure 13. Nu vs. T_{inlet} the 7 × 21 cube array microchannel.

Figure 14 shows the heat transfer and friction factor results with variation of input power to the microchannel with a configuration of 7 rows and 21 columns of VG bars. To study the effect of test parameters, the data has been statistically analyzed and it has been found that the data is normally distributed and the heat flux and Reynolds number and heat flux variation has a significant effect on the heat transfer rate while the change in inlet temperature of the fluid does not have a significant effect. The Nusselt number can be seen to increase significantly after Reynolds number of 100. In the range of Reynolds number tested, an increase in 10 watts gave about 15 % increase at Re ≈ 100 and 11 % at Re ≈ 500 in Nusselt number.

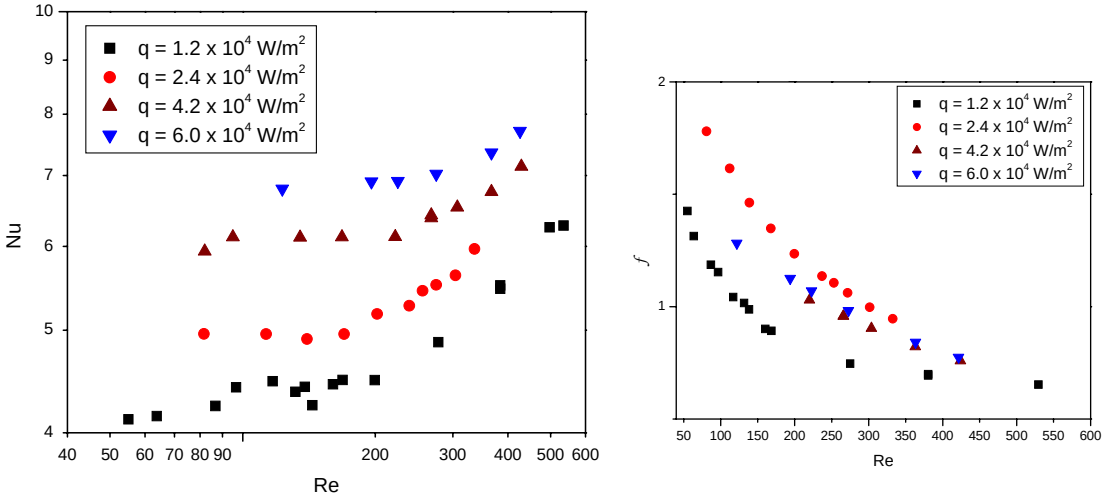

Figure 14. Nu and *f* vs. Re for the 7 × 21 cube array microchannel.

In Figure 15, the near-linear effect of heat flux level on Nusselt number can be seen for a fixed inlet temperature of 20°C. The Reynolds number was kept constant for each of the four different cases. It was observed that at fixed heat flux, the Nusselt number changed by about 5% with change in Reynolds number of 100 within the range of 100-500.

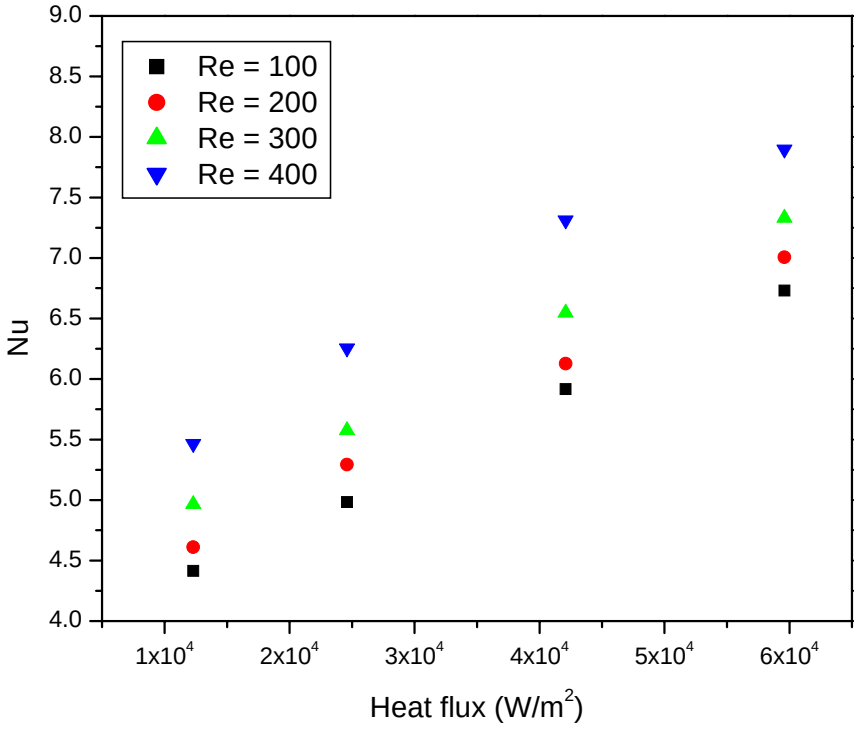

Figure 15. Nu vs. q for the 7 × 21 cube array microchannel.

We define the Colburn *j* factor as a measure of heat transfer

$$j = \frac{Nu}{\mathrm{RePr}^{0.4}} \tag{10}$$

The Colburn *j* factors obtained from the experiment are found to be larger than those obtained by steady and unsteady simulation models of Zhang et al[19], confirming that the overall heat transfer was improved. Figure 16 shows the Colburn *j* factors for four heat fluxes used in the experiments.

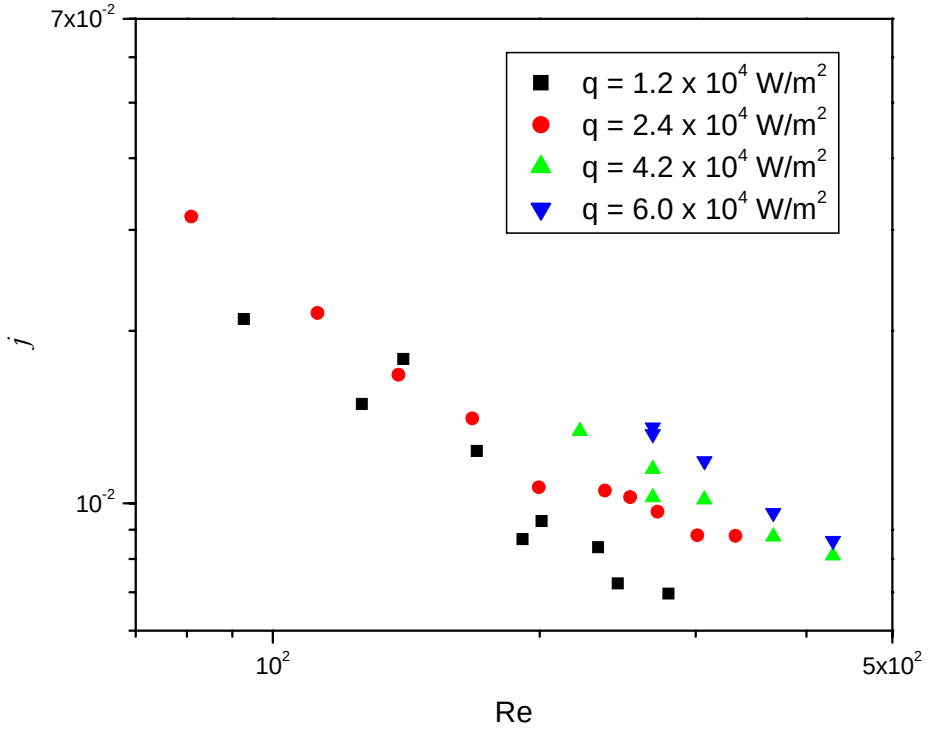

Figure 16. Colburn *j* factor comparison for the 7 × 21 cube array microchannel.

In Figure 17, the friction factor is plotted against the Reynolds number for the 7 × 21 cube array microchannel. The friction factor for all the cases is seen to follow a certain trend. The product *f*Re and temperature ratio response with change in Reynolds number are shown in Figures 18 and 19.

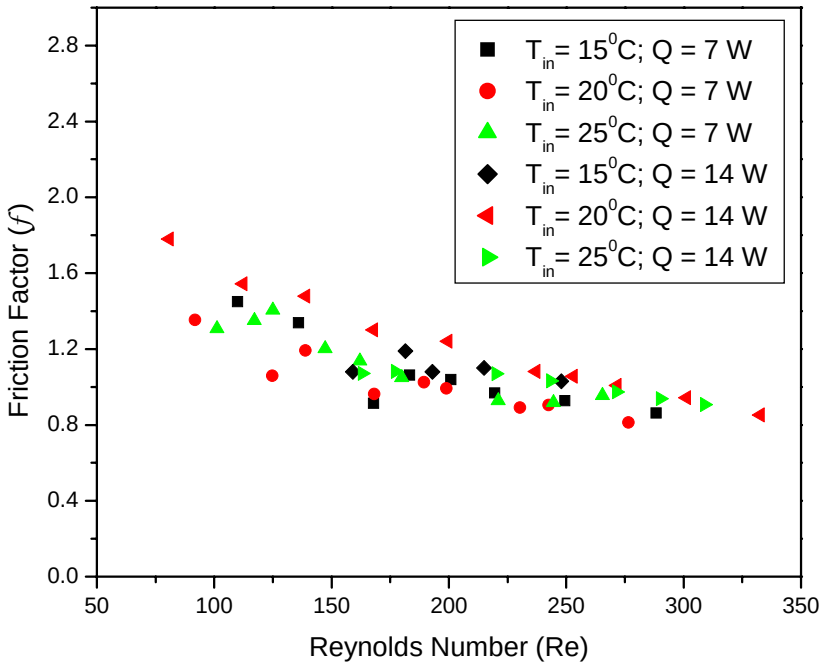

Figure 17. f vs. Re for the 7 × 21 cube array microchannel.

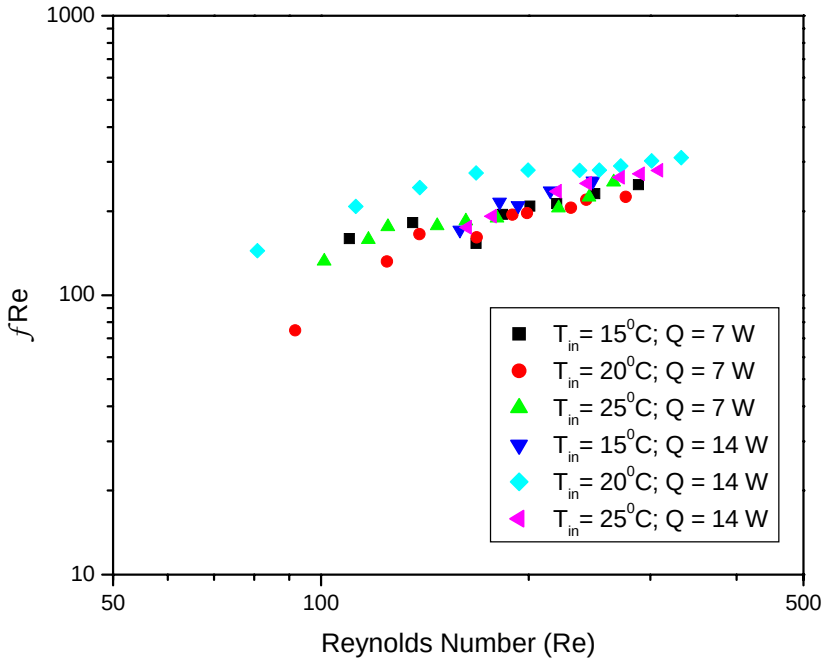

Figure 18. *fRe* vs. Re for the 7 × 21 cube array microchannel.

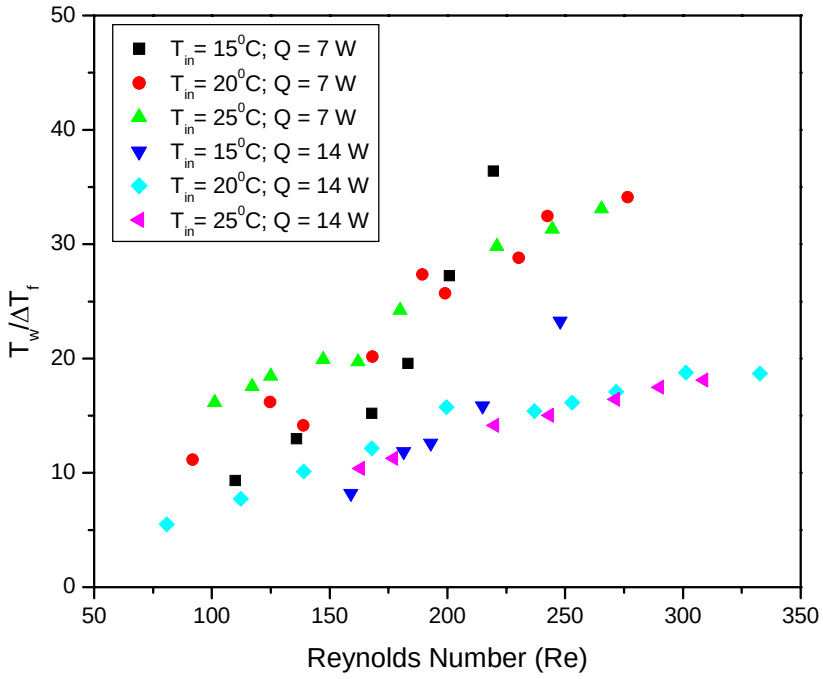

Figure 19. Temperature ratio vs. Re the 7 × 21 cube array microchannel.

Figure 20 shows the surface temperature variation along the length of the channel. It can be seen that at high Re the surface temperature is decreased, which suggests more heat transfer. But the Nusselt number variation is not much. This may be attributed to the fact that the heat transfer is not only taking place by convection but also by conduction. Thus, conduction as well as convection heat transfers may be increasing by similar proportions when the Reynolds number is increased.

Figure 21 shows the inlet, outlet and wall temperature distributions along the test section with 7 × 21 cube array. The inlet temperature was kept constant at 20 ^{o}C and the heat input was maintained at 7 Watts. Results at Re of 200 and 300 are given. It can be seen that the wall temperature was decreased along flow direction at higher Reynolds number. While the change in Reynolds number had an insignificant effect at the entrance of the test section, there was 5 % decrease in the wall temperature at a distance of 40 mm from the entrance.

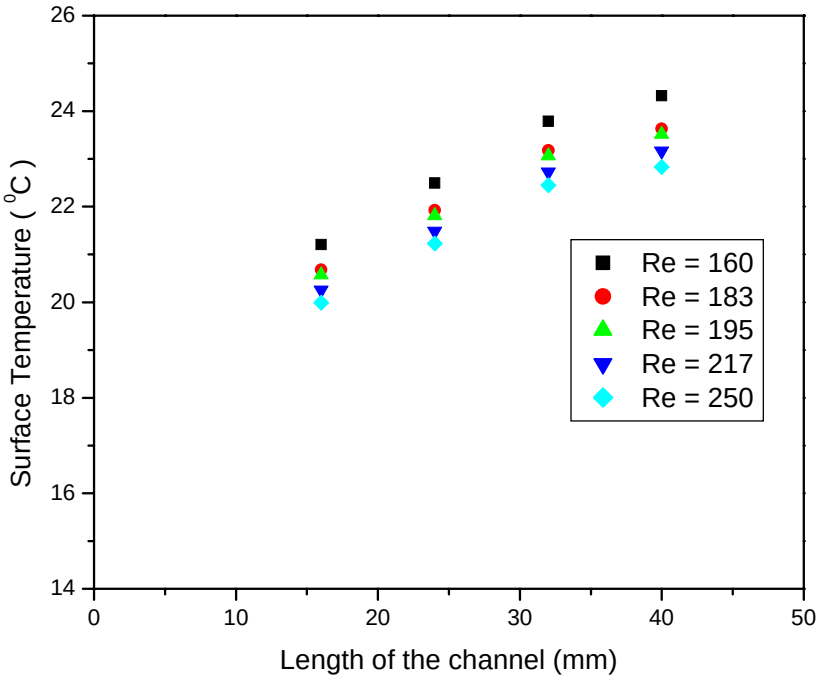

Figure 20. Variation of surface temperature along the 7 × 21 cube array microchannel.

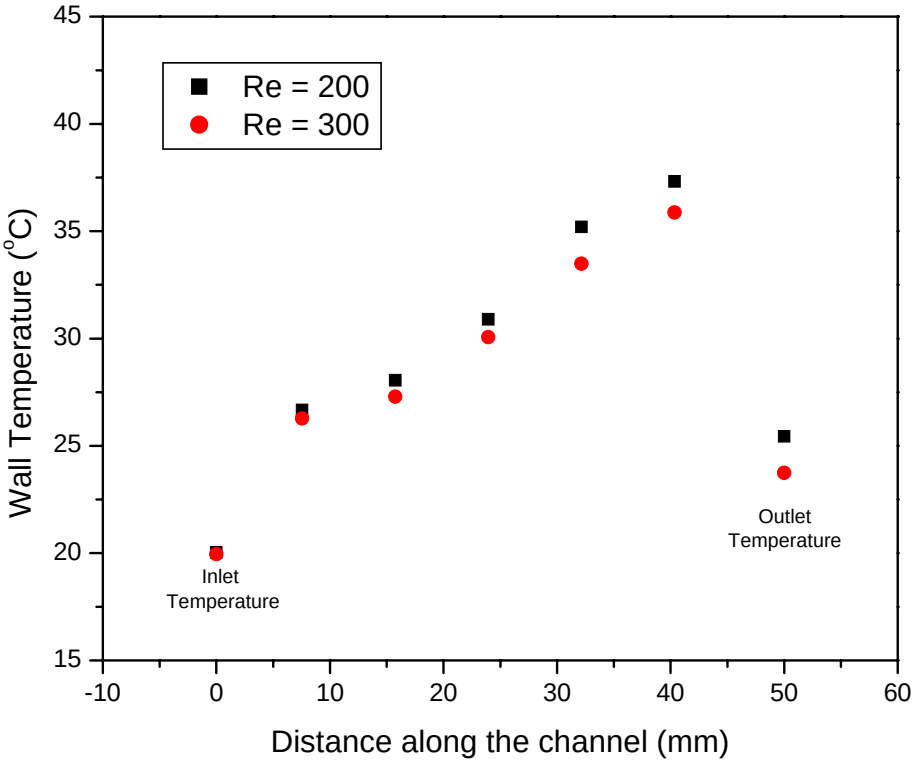

Figure 21. Variation of surface temperature along the 7 × 21 cube array microchannel.

Figure 22 shows the temperatures change with time at a distance of 15 mm (a) and 40 mm (b) for Reynolds number at 200 and 500. Attempts were made to verify if there is an oscillation of the wall temperatures. The temperature was recorded for every 100 milliseconds. There were some fluctuations observed and which were of a magnitude of ± 0.5% from the average value. Most of them were found to be random fluctuations rather than periodic.

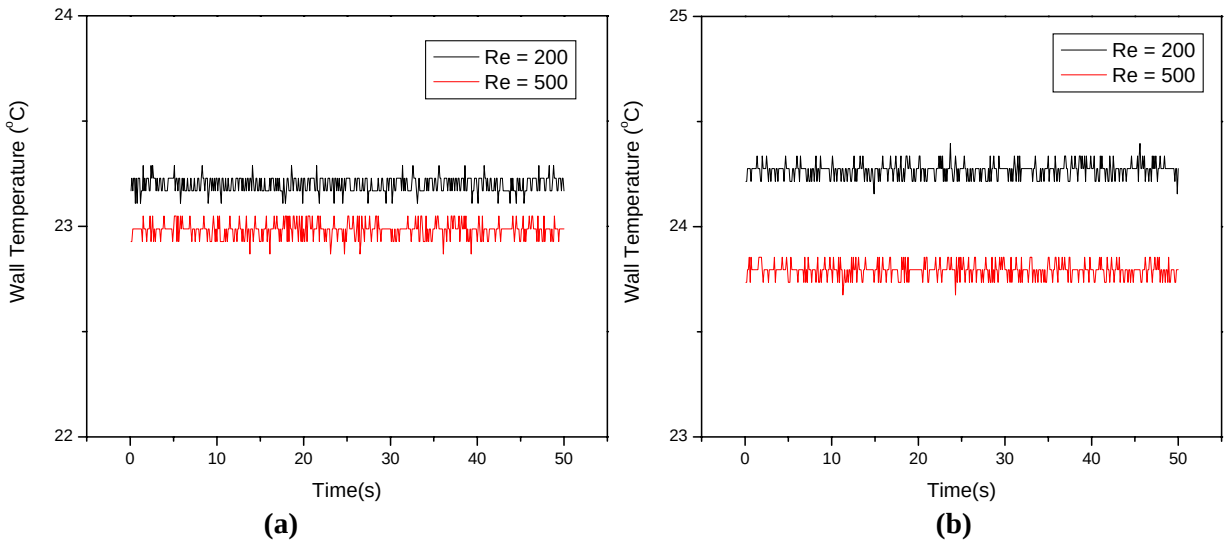

Figure 22. Variation of temperature with time.

2.4 Conclusions from the experimental study

Heat transfer study with single- and multi-row VG-equipped microchannels resulted in following findings:

For a single-raw VG-equipped microchannel the heat transfer and wall temperature distribution in microchannel are improved compared with a channel without VG bars, while the flow resistance is larger.

For a multi-raw VG-equipped microchannel:

- increase of inlet fluid temperature results in increased Nusselt number
- the Nusselt number is almost the same for the different heat input conditions with the same inlet fluid temperature

- the Nusselt number increases significantly when the Reynolds number increases above 100
- the Nusselt number increases almost linearly with increasing heat flux to the microchannel
- experimentally obtained Colburn *j* factors are larger than those obtained by steady and unsteady simulation models of Zhang et al[19], confirming that the overall heat transfer was improved
- with increasing Reynolds number the microchannel surface temperature is decreasing
- the wall temperature was decreased along flow direction at higher Reynolds number, while the change in Reynolds number had an insignificant effect at the entrance of the microchannel
- no microchannel wall temperature oscillations were observed under studied range of experimental conditions

3 Numerical Study

3.1 Mathematical models and numerical methods

3.1.1 Computational domain

Three different arrays of VG bars in the same channel were used to numerically study the water flow and heat transfer in a 3-D microchannel, with $H = W = 800$ μm, $D_h = 800$ μm, and the channel length over the hydraulic diameter ratio of $L/D_h = 5$. Figure 23 (a), (b) and (c) presents the channel geometry with the 1, 2 and 4 VG bars, respectively. The upstream and downstream points are defined for tracing the history value of flow properties with time.

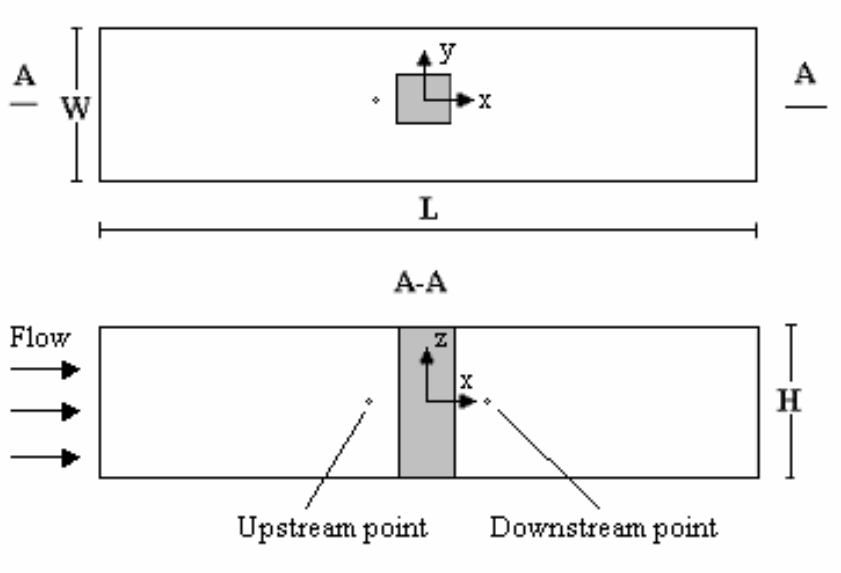

(a)

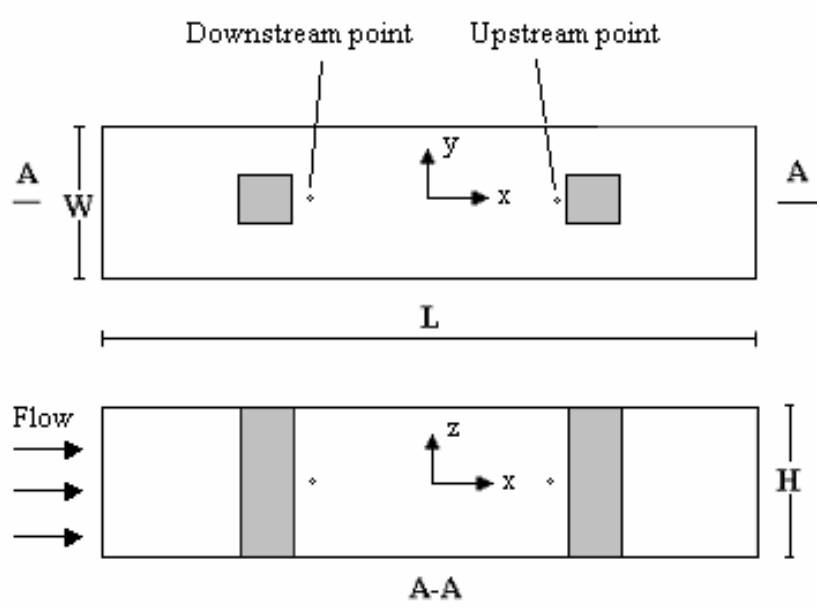

(b)

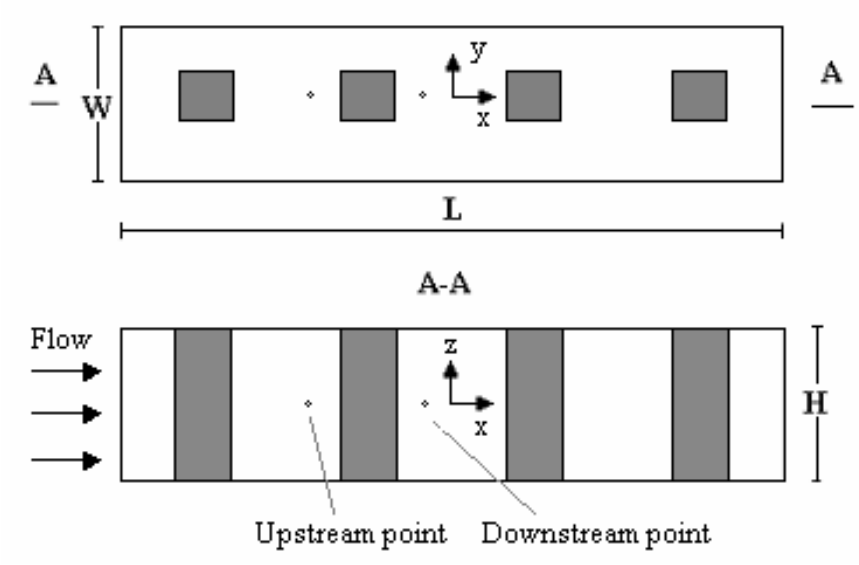

(c)

Figure 23. Microchannel geometry: a) 1-bar array; b) 2-bar array; c) 4-bar array.

3.1.2 Governing equations

Three-dimensional continuity, momentum and energy equations in Cartesian tensor notations are described as follows:

Continuity equation

$$\frac{\partial(\rho u_j)}{\partial x_j} = 0 \tag{11}$$

Momentum equation

$$\frac{\partial(\rho u_i)}{\partial t} + \frac{\partial(\rho u_j u_i)}{\partial x_j} = -\frac{\partial p}{\partial x_j} + \frac{\partial}{\partial x_j}\left(\mu \frac{\partial u_i}{x_j}\right) + \frac{\partial}{\partial x_j}\left(\mu \frac{\partial u_j}{x_i}\right) - \frac{2}{3}\frac{\partial}{\partial x_i}\left(\mu \frac{\partial u_k}{x_k}\right) \tag{12}$$

Energy equation

$$\frac{\partial(\rho C_p T)}{\partial t} + \frac{\partial(\rho C_p u_j T)}{\partial x_j} = \frac{\partial}{\partial x_j}\left(k \frac{\partial T}{\partial x_j}\right) + \mu \dot{\gamma}^2 \tag{13}$$

Where

$$\dot{\gamma}^2 = 2\left[\left(\frac{\partial u}{\partial x}\right)^2 + \left(\frac{\partial v}{\partial y}\right)^2 + \left(\frac{\partial w}{\partial z}\right)^2\right] + \left(\frac{\partial u}{\partial y} + \frac{\partial v}{\partial x}\right)^2 + \left(\frac{\partial u}{\partial z} + \frac{\partial w}{\partial x}\right)^2 + \left(\frac{\partial v}{\partial z} + \frac{\partial w}{\partial y}\right)^2 \tag{14}$$

3.1.3 Boundary conditions

The schematic for boundary conditions is shown in Figure 24. The boundary conditions are described as follows:

Inlet and outlet: Periodic conditions, specifying the mass flow rate (Q = *constant*) and the temperature.

Wall: All the surfaces are treated as no-slip boundaries. And the walls were adiabatic $q'' = 0$, except that the bottom wall is heated with constant heat flux $q'' = const$.

The velocities, pressure and temperature in the streamwise direction of the computational domain is considered for periodic boundary conditions. The assumption of periodicity implies that the velocity components repeat themselves in space as follows:

$$u_i(\vec{r}) = u_i(\vec{r} + \vec{L}) = u_i(\vec{r} + 2\vec{L}) = \cdots \tag{15}$$

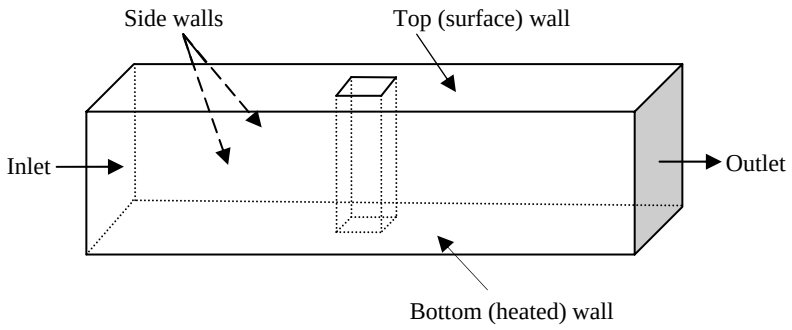

Figure 24. Schematic for boundary conditions

The pressure is not periodic. Instead, the pressure drop between modules is periodic:

$$\Delta p = p(\vec{r}) - p(\vec{r} + \vec{L}) = p(\vec{r} + \vec{L}) - p(\vec{r} + 2\vec{L}) = \cdots \tag{16}$$

Similarly, the temperature drop between modules is periodic:

$$\Delta T = T(\vec{r}) - T(\vec{r} + \vec{L}) = T(\vec{r} + \vec{L}) - T(\vec{r} + 2\vec{L}) = \cdots \tag{17}$$

Where $\vec{r}$ is the position vector and $\vec{L}$ is the periodic length vector of the domain considered.

3.1.4 Model description

The time-dependent governing Navier-Stokes equations were solved with finite volume method. The continuity, momentum and energy equations were solved by second order upwind implicit scheme using an unsteady laminar solver, and the pressure-velocity coupling was dealt with by SIMPLEC algorithm. For the conjugate heat transfer problem, the same energy equation is used for the fluid domain as well as the solid domain with high conductivity and zero velocity within the VG bars. To avoid the divergence, the under-relaxation technique was applied in all dependent variables. In the investigation, the under-relation factor for the pressure was 0.7, that for the velocity components was 0.9, and that for energy conponent was 0.9. In the segregated solution method, each discrete governing equation was linearized

implicitly with respect to that equation's dependent variable. The convergence criterion for residuals was set to 10^{-6} for all the continuity, momentum, and energy equations.

3.1.5 Mesh independence study

In order to achieve a grid independent solution for the microchannel simulations, computations have been performed at three different meshes 16 x 16 x 80, 20 x 20 x 100, and 32 x 32 x 160 at Reynolds number of 300 by comparing the values of averaged Nusselt number on the heated wall and the *f*Re* number. The Nusselt number shows variations of 9.9 % and 4.1 % while the *f*Re* number reveals variations of 4.0 % and 1.0 % for 16 x 16 x 50 and 20 x 20 x 100 grids respectively with respect to the grid size of 32 x 32 x 160. The Nusselt number and *f*Re* variation with mesh number can be found in Figure 25 (a) and (b) respectively. Consequently the mesh size of 20 x 20 x 100 was selected as grid independent result and was used for all the simulations. Figure 26 shows the mesh used in the simulations with the domain with one VG bar.

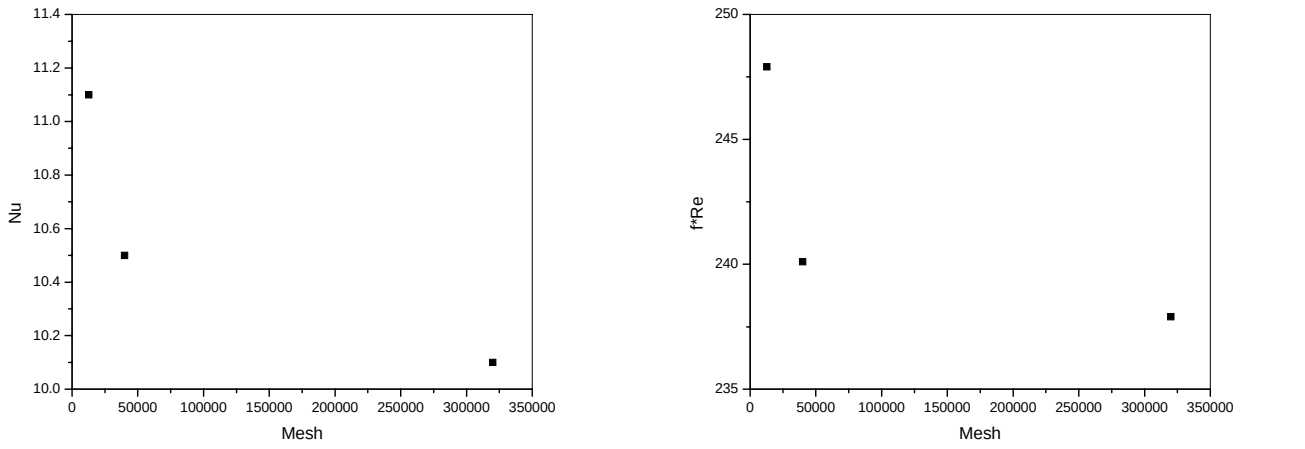

Figure 25. (a) Nusselt number versus mesh number; (b) *f*Re* number versus mesh number

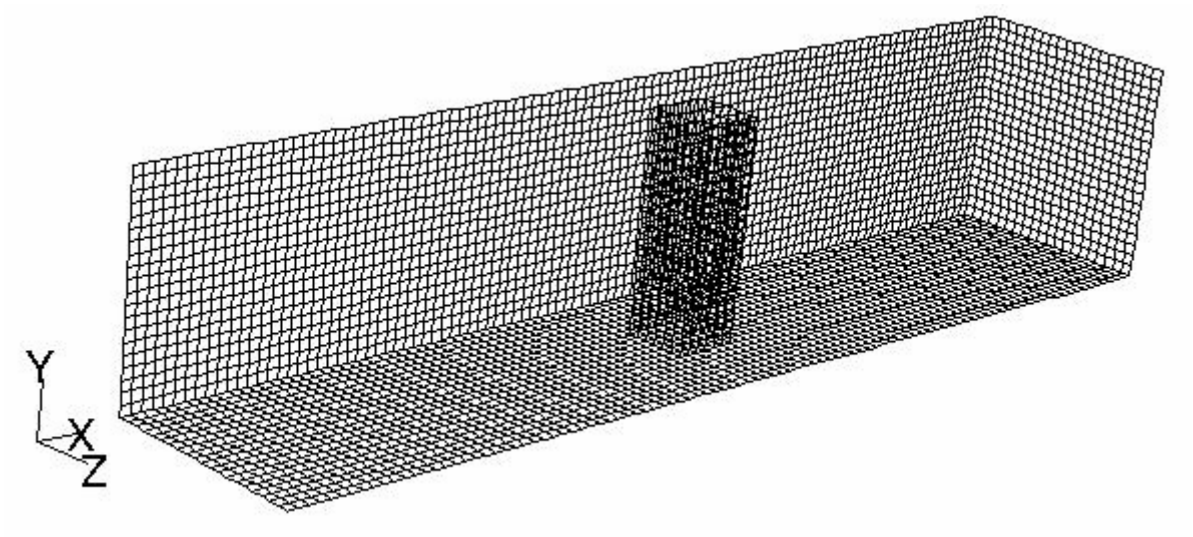

Figure 26. Mesh of the one bar array domain.

3.1.6 Fluid Properties

The water properties used in the simulations are tabulated in table 1. The constant properties were used in the computational simulations.

Table 1 Properties of water used in simulations

Density	Viscosity	Heat conductivity	Specific heat
998.2 (kg/m^3)	0.001003 (kg/m·s)	0.6 (w/m·k)	4182 (j/kg·k)

3.1.7 Model Validation

The present numerical model has been validated by comparing the Nusselt number and pressure drop with the experimental results available in the literature [29, 30]. The comparison of Nusselt number between numerical solutions and experimental results provided by Lee et al [29] is shown in Figure 27 using the three-dimensional numerical model at steady state. Figure 28 presents the comparison of the numerical solutions with experimental data of pressure drop in microchannels by Qu and Mudawar [30]. The numerical results for Nusselt number and pressure drop are in good agreement with the experimental

results at low Reynolds number. However, when Reynolds number is larger than 1500, the numerical results of Nusselt number and pressure drop are obviously lower than experimental results. The reason for this is due to the fact that the laminar model was used to simulate the fluid flow and heat transfer whereas the flow may become turbulent at high Reynolds number for microchannels.

To get more confidence in the present simulation, the numerical model has also been tested for the flow past a circular cylinder placed in an otherwise undisturbed uniform cross-flow. The Strouhal number in the near wake of the circular cylinder at Reynolds number of 100 was found to be 0.173 well matching with the Srouhal number of 0.165 from published experimental results [32].

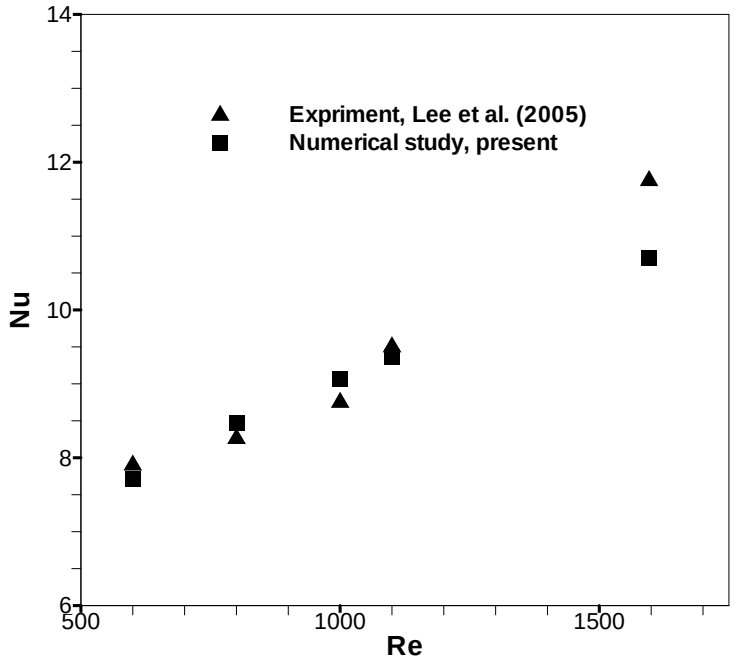

Figure 27. Comparison of Nusselt number between numerical results and experimental data

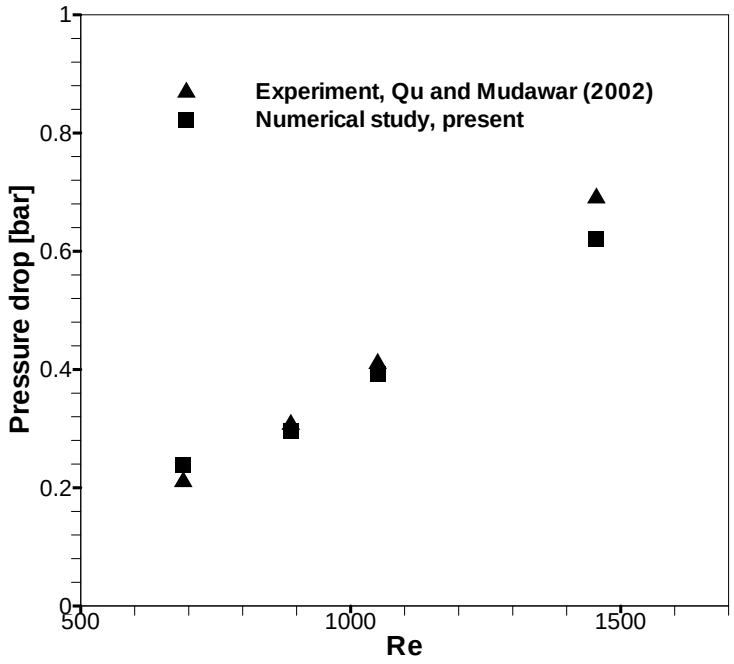

Figure 28. Comparison of pressure drop between numerical results and experimental data

3.2 Numerical results and discussion

The simulations have been carried out at several different Reynolds numbers corresponding to different VG-bar arrays.

Numerical data are calculated using hydraulic diameter defined as:

$$d_h = \frac{4A_c}{P} \tag{18}$$

The Reynolds number, *Re*

$$\mathrm{Re} = \frac{\rho u d_h}{\mu} \tag{19}$$

The Nusselt number, *Nu*

$$Nu = \frac{h d_h}{k} \tag{20}$$

And the friction factor, *f*

$$f = \frac{\Delta P d_h}{\frac{1}{2}\rho u^2 L} \tag{21}$$

Where Δp_x is the axial pressure drop.

The Strouhal number, *St*

$$St = \frac{ND_h}{V} \tag{22}$$

Where, *N* is the frequency of velocity oscillations and *V* is the velocity.

The averaged friction factor and Nusselt number have been tabulated and shown in Table 2. The tabulated friction factors and Nusselt numbers have been normalized with respect to the corresponding values in the flow of the channel without bars (later called smooth channel). From the table one can see that the friction factors for the microchannel with bars are over 3 times larger than those of the microchannels without bars and the Nusselt numbers with bars are significantly enhanced by 3~5 times at Reynolds number of 300 and 400.

The effect of the number of VG bar(s) on the normalized friction factors and Nusselt number can be more clearly shown in Figure 29 (a) and (b). The normalized Nusselt number increased with increasing number of VG bars at Reynolds number of 300. However, the normalized Nusselt number decreased for the channel with the number of bars varied from 2 to 4 at Reynolds number of 400. The normalized friction factor increased with the number of bars for both Reynolds number of 300 and 400. The normalized friction factor increased more when the number of bars changed from 1 to 2 than when the number of bars changed from 2 to 4.

Table 2. The averaged friction factors and Nusselt number in single microchannel with different VG-bar arrays and various Reynolds number.

Bar(s)	D_h (μm)	Re	f_{bars} / f	Nu_{bars} / Nu
1	800	300	3.03	3.04
1	800	400	3.59	3.80
2	800	200	3.62	2.93
2	800	300	4.71	3.74
2	800	400	5.78	4.88
4	800	300	5.23	4.38
4	800	400	6.01	4.74

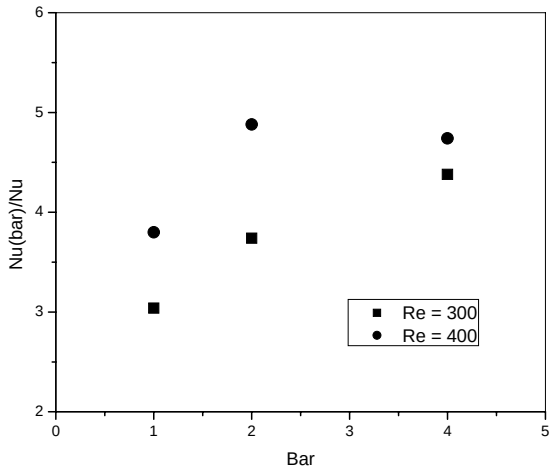

(a)

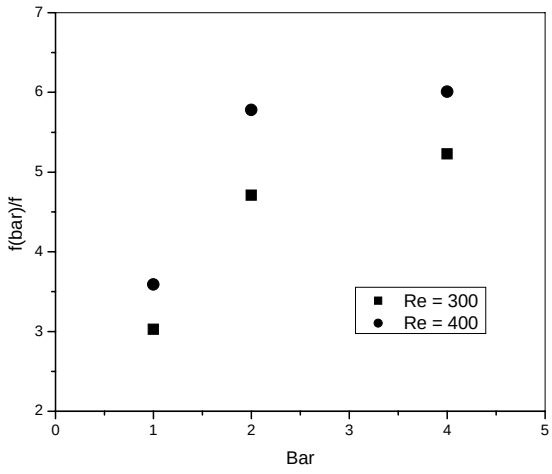

(b)

Figure 29. (a) Non-dimensional Nusselt number for the microchannel with different VG-bar arrays at Reynolds number of 300 and 400; (b) Non-dimensional friction factor for the microchannel with different VG-bar arrays at Reynolds number of 300 and 400;

Table 3 presents the frequency of velocity oscillation and Strouhal number for various Reynolds numbers and bar-arrays. The frequency increased with the increase of Reynolds number. The frequency with 4 bars was larger than the frequency with 2 bars, which was larger than that of 1-bar array. However, the Strouhal numbers for different cases were very close only ranging from 0.99 to 1.1.

Table 3 The Frequency and Strouhal number at different Reynolds number and various VG-bar arrays.

Bar(s)	$\mathbf{D_h}$ (μm)	**Re**	**N** (frequency)	**St** (Strouhal)
1	800	300	0	0
1	800	400	653.59	1.05
1	800	600	925.93	0.99
2	800	200	344.83	1.1
2	800	300	476.19	1.02
2	800	400	chaotic	N/A
2	800	500	chaotic	N/A
4	800	300	483.09	1.03
4	800	400	chaotic	N/A

Figures 30 (a), (b), and (c) show the time traces of velocity at Re = 300, 400, and 500 respectively for upstream and downstream points shown in Figure 23 for the channel with 2 bars. The velocity was periodically changing with time. The unsteady and oscillating behavior of flow was found. The frequency of velocity can be easily calculated at Re = 300 for the channel with 2-bar array. But the flow was chaotic and the frequency was uncertain at Reynolds number of 500. From these figures, we conclude that the velocity at the upstream point is always higher than that at downstream point, but they have the

same frequencies of oscillation. The oscillating amplitude of velocity of higher Reynolds number is larger than that of lower Reynolds number.

Figure 31 and Figure 32 show the time traces of wall temperature and Nusselt number respectively for the central point of bottom wall at Re = 300 and 400 with 2-bar array. The oscillating behavior of wall temperature as well as Nusselt number with time was found. The wall temperature increased and the Nusselt number decreased with time, however, after four seconds, the averaged temperature and Nusselt number became constant. The averaged Nusselt numbers were about 10.1 and 13.2 for Reynolds number of 300 and 400 respectively. Considering that the Nusselt number was only about 2.7 for the channel without VG bar, the heat transfer in microchannel with VG bars was significantly enhanced due to the unsteady and oscillating flows generated by the VG bars.

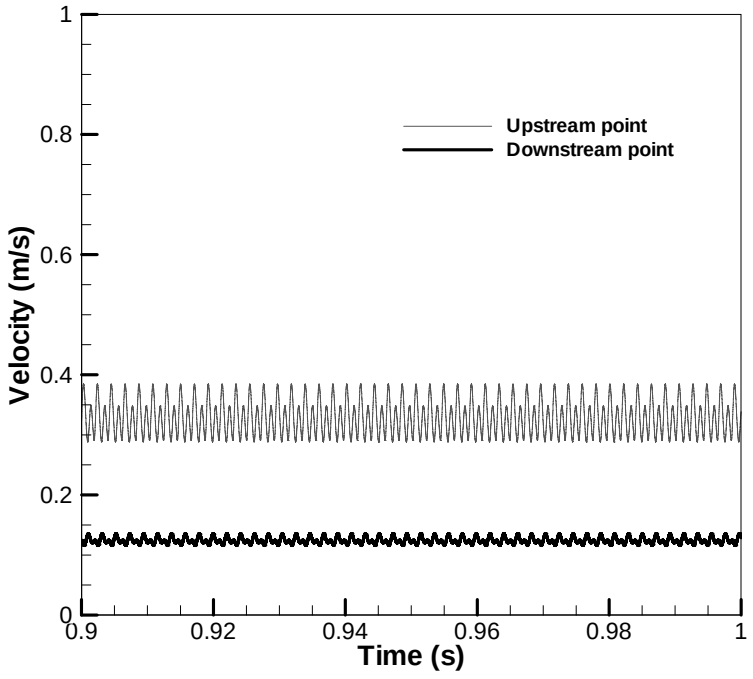

(a)

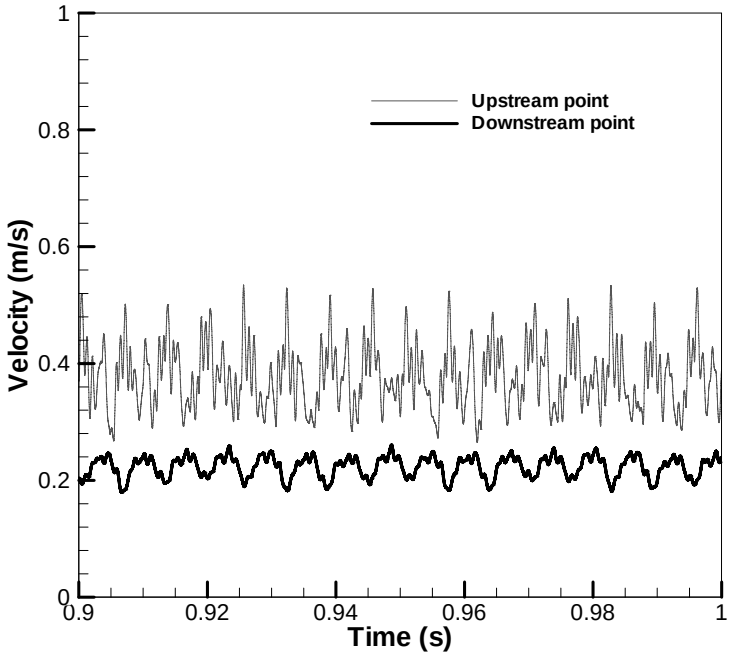

(b)

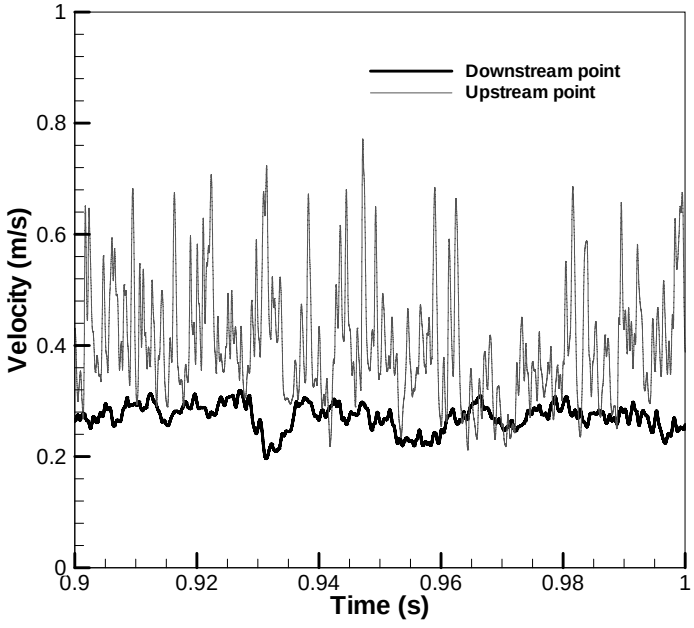

(c)

Figure 30. History traces of the velocity for upstream and downstream points (2 bars). (a) Re = 300; (b) Re = 400; (c) Re = 500.

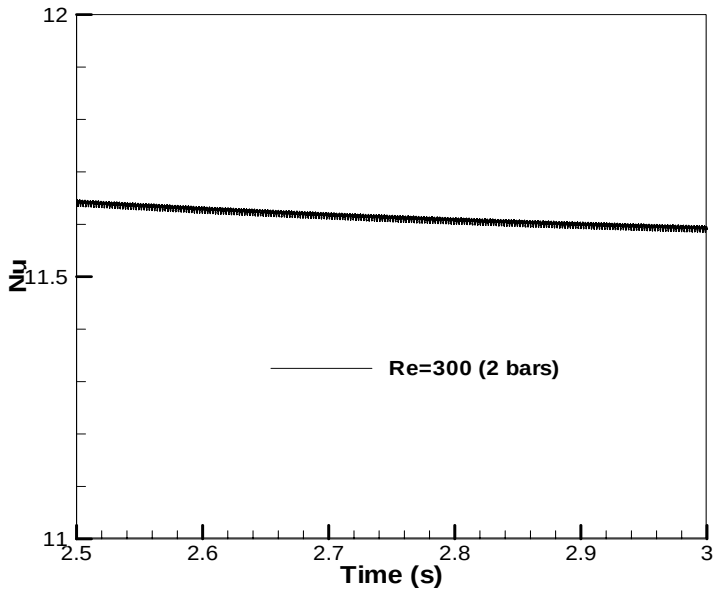

(a)

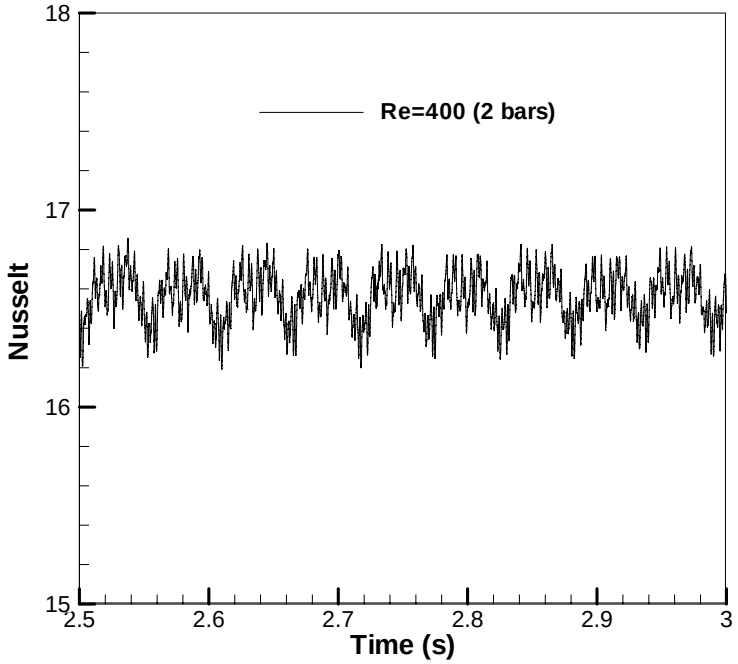

(b)

Figure 31. History traces of averaged Nusselt number at bottom plate for the microchannel with 2-bars array. (a) Re = 300; (b) Re = 400.

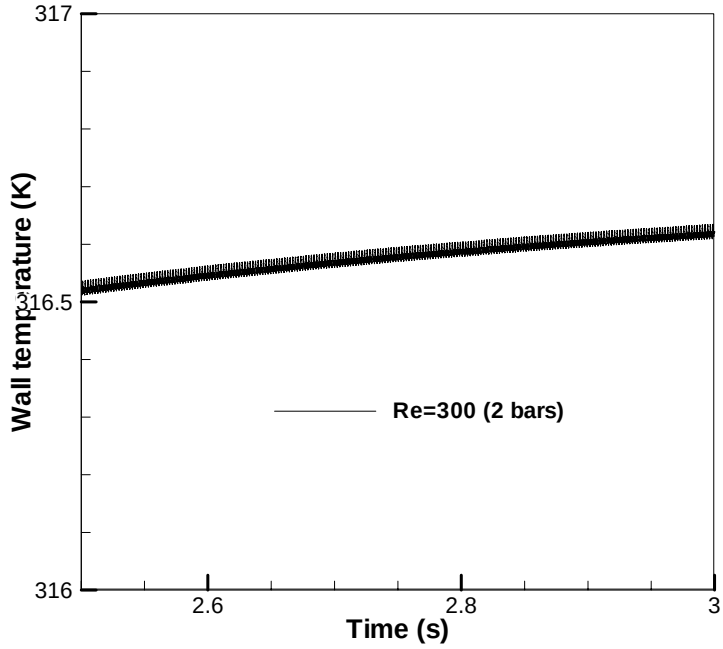

(a)

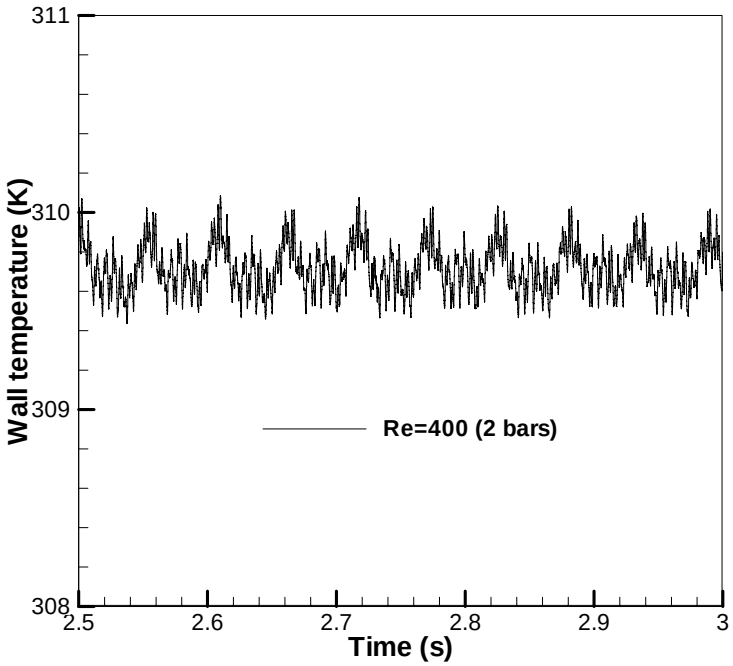

(b)

Figure 32. History traces of averaged temperature at bottom wall for the microchannel with 2-bars array. (a) Re = 300; (b) Re = 400.

Figure 33 and Figure 34 respectively show the contours of streamwise and transverse component of velocity with different bar-arrays at Reynolds number of 400. The strongly unsteady and oscillating flows were found for the channels with various bar-arrays. Results indicated that the boundary layers were interrupted and became thinner near the VG bars, at the same time the large-scale unsteadiness was found inside the microchannels. The strengths of vorticity with 1-bar and 2-bar arrays were weaker than that of the channel with 4 bars.

The contours of transverse, spanwise, and streamwise components of vorticity are shown in Figure 35 to Figure 37. It can be seen that the flow vorticity upstream of the bar is considerably stronger than the vorticity downstream of the bar. The unsteady natures of the flow were indicated from the pattern of vorticity distribution. Figure 35 shows the contours of spanwise component of vorticity. It is obvious to find the formation of separating shear layers at the leading edges, but the shear layers do not roll up to form large-scale vertical structure behind the bars. The transverse component of vorticity is presented in Figure 36, it also shows that the upstream vorticity is much stronger than downstream vorticiy. Although the vorticity in transverse direction was weak, it may have played an important role in enhancing heat transfer due to considerable increase in Nusselts number shown in Table 2. From Figures 35 and 36, the channel with 4-bar array has the strongest vorticity. The behavior of streamwise vorticity can be found form Figure 37, it also shows the channel with more bars has stronger vorticity.

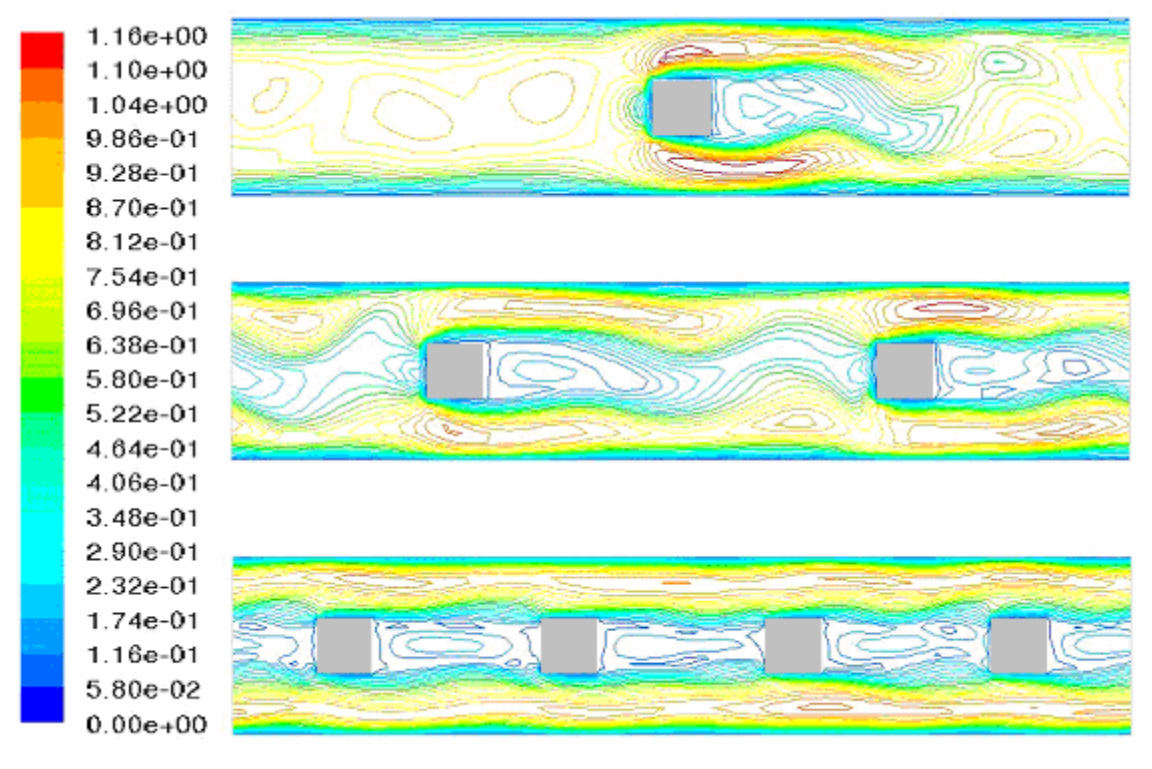

Figure 33. Contours of spanwise component of velocity with different bar-arrays (*Re* = 400, D_h = 0.8mm, *time* = 0.8s)

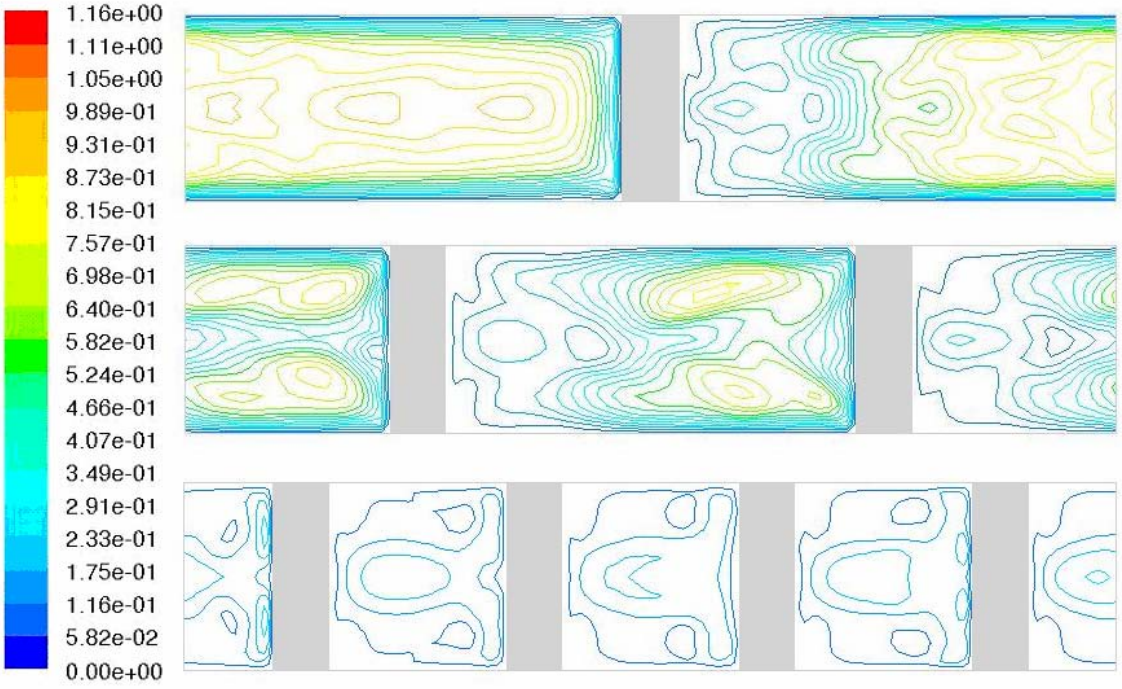

Figure 34. Contours of transverse component of velocity with different bar-arrays (*Re* = 400, D_h = 0.8mm, *time* = 0.8s)

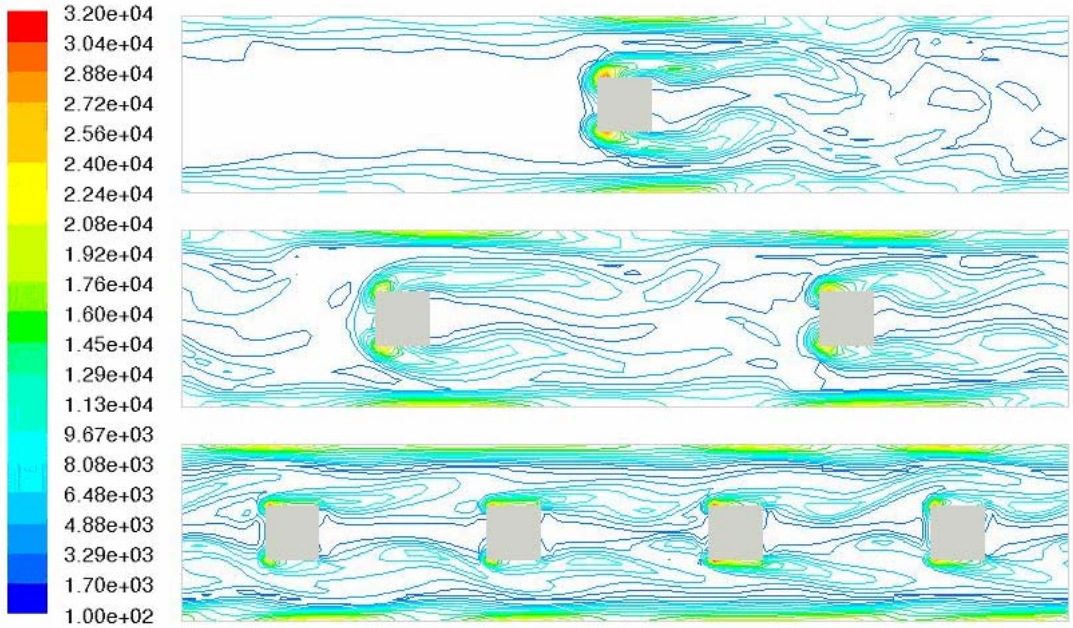

Figure 35. Contours of spanwise component of vorticity with different bar-arrays (*Re* = 400, D_h = 0.8mm, *time* = 0.8s)

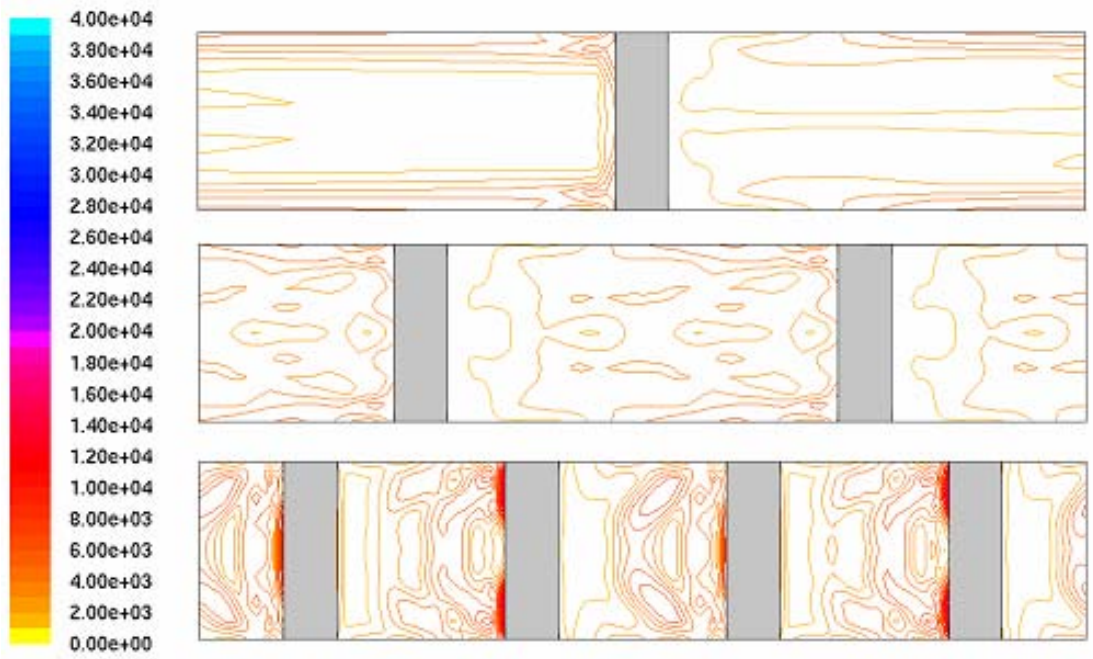

Figure 36. Contours of transverse component of vorticity with different bar-arrays (Re = 300, D_h = 0.8mm, time = 0.18s)

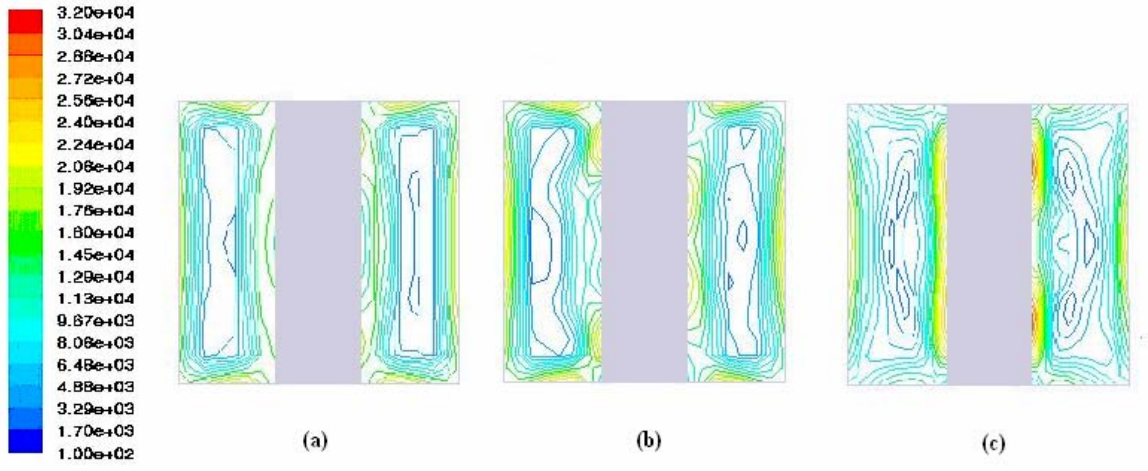

Figure 37. Contours of streamwise component of vorticity at mid plane with different bar-arrays (*Re* = 400, *time* = 0. 8s): a) 1-bar array; b) 2-bar array; c) 3-bar array.

Figures 38 and 39 present the temperature contours of bottom wall with 1-bar and 4-bar arrays respectively. Figure 41 and Figure 42 show the three-dimension temperature contours at the bottom wall and the surfaces of bars. Although the downstream and upstream velocities of the channel with 4 bars were weak compared with other channels, the temperature of bottom wall of the channel with 4 bars was more uniform and lower than that with one bar due to high heat transfer resulted from its strong vorticity and mixing. This means the channel with more bars has enhanced the heat transfer better. The channel with 4-bar array can sustain larger heating flux at bottom wall. Figure 40 shows the temperature contour of bottom wall with 2-bar array but the heat flux was set to 200,000 w/m^2, while the heat flux was set to 50000 w/m^2 for the channel with 1 and 4 bars. With this heat flux the temperature of bottom wall was significantly increased and more uneven, especially at the edges of the bottom wall.

It is interesting to find that the temperature at the region near the bars was lower than that at the other area of the heating wall. The VG bars improved the heat transfer in microchannels due to the unsteady and oscillating fluid flow.

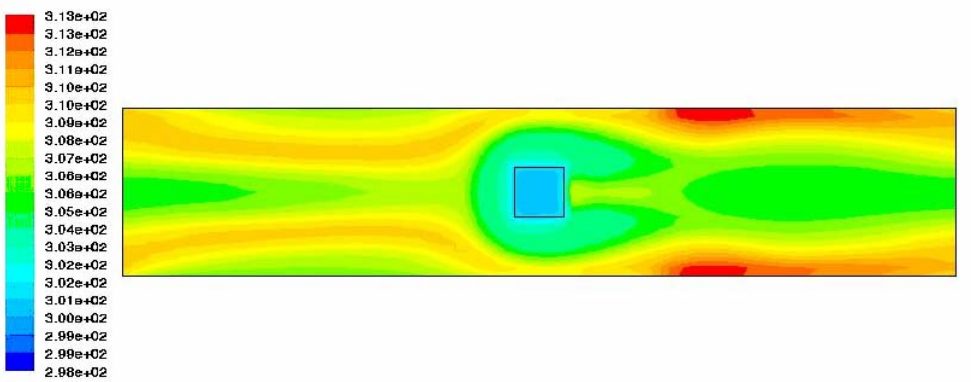

Figure 38. The temperature contour at bottom plane (*Re* = 400, 1 bar, *time* = 0.8 sec, *q* = 50000 w/m^2)

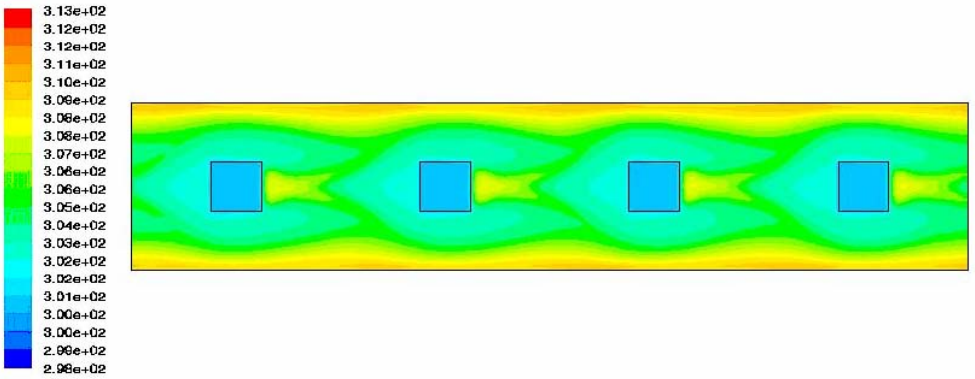

Figure 39. The temperature contour at bottom plane (*Re* = 400, 4 bars, *time* = 0.8 sec, *q* = 50000 w/m^2)

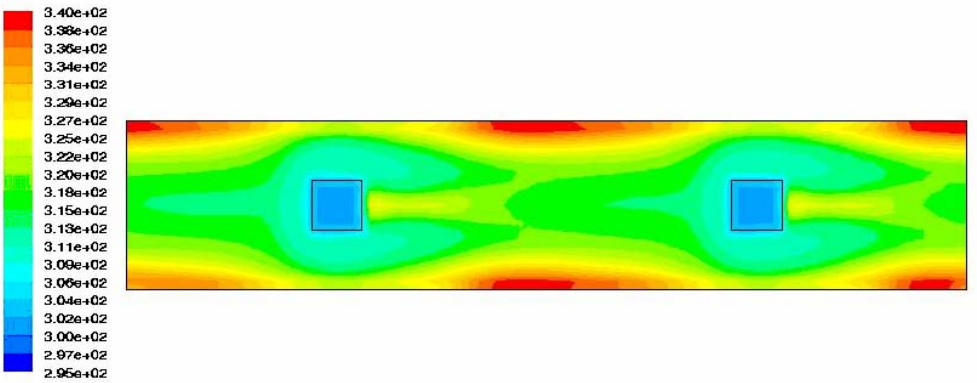

Figure 40. The temperature contour at bottom plane (*Re* = 400, 2 bars, *time* = 0.8 sec, *q* = 200000 w/m^2)

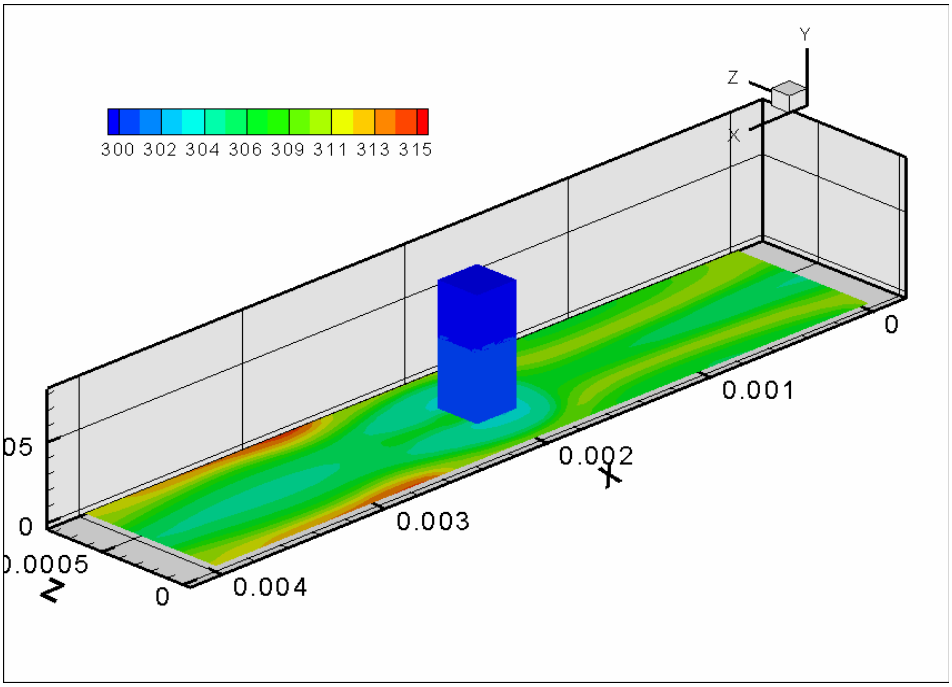

Figure 41. The 3-D temperature contour at bottom plane and surfaces of bar (*Re* = 400, 1 bar, *time* = 0.8 sec, *q* = 50000 w/m^2)

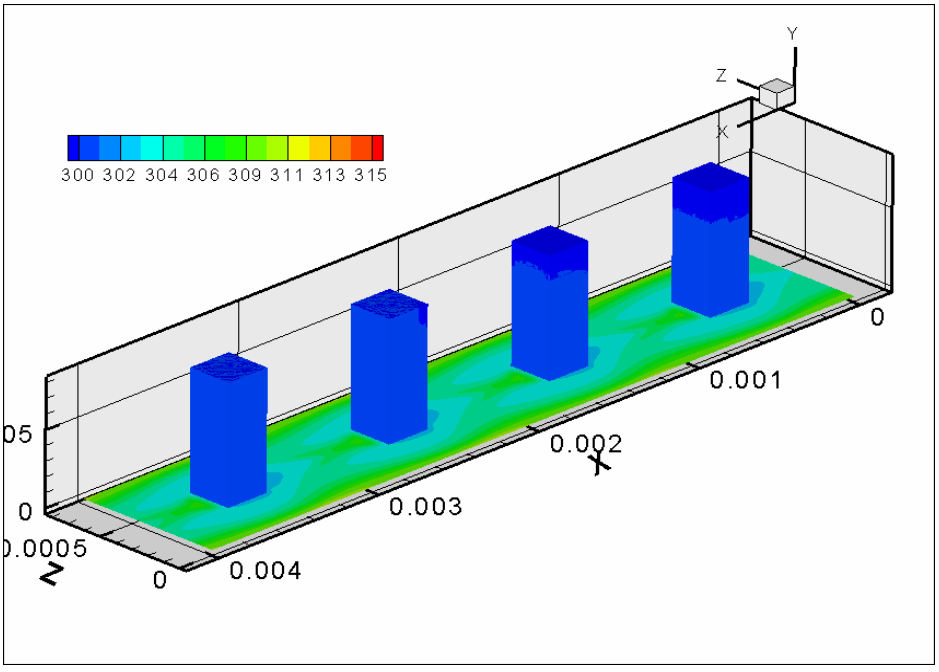

Figure 42. The 3-D temperature contour at bottom plane and surfaces of bar (*Re* = 400, 4 bars, *time* = 0.8 sec, *q* = 50000 w/m^2)

3.3 Conclusions from the numerical study

Microchannel with VG bars can provide high heat transfer surface area per unit volume and alter the fluid dynamics to enhance mixing. Numerical study of fluid flow and heat transfer in the microchannel with VG bars resulted in following findings:

- The flow in microchannel was found to be unsteady and oscillating at Reynolds number equal to or larger than 300 with 2 bars and 4 bars. For the microchannel with 1 bar the flow was found to be naturally steady at Reynolds number of 300. At Reynolds number of 500 with 2 bars, the flow in the microchannels could become chaotic.
- For most of the microchannels with bars, the friction factor was more than 3 times larger than that for the microchannels without bars at the same Reynolds number.
- The larger the Reynolds number and the more the number of VG bars, the stronger the unsteadiness and oscillations of the flows
- With increasing Reynolds number the averaged temperature of heated wall was decreased
- The oscillating behavior of velocity, averaged temperature on the bottom wall, and Nusselt number was found at Reynolds number of 300 or larger for the channel with 2 or 4 bars, and at Reynolds number of 400 or larger for the channel with 1 bar.

4. Publications stemming from this research effort

- Mo, H. L., Prattipati, R. C. and Lin, C. X., "Experimental Study of Liquid Flow and Heat Transfer in Microchannels with In-Line Array of Cubes", 2005 Summer Heat Transfer Conference, HT 2005-72830, San Francisco, CA, July 17-22, 2005.

- Ye, C. M. and Lin, C. X., Numerical study of liquid flow and heat transfer in single microchannel with in-line array of bars, Proceedings of AIAA-2006, AIAA/ASME Joint Thermophysics and Heat Transfer Conference, 2006, San Francisco, CA. (AIAA-2006-3623)

- Prattipati, R. C. and Lin, C. X., Experimental Investigation of Heat Transfer in a Microchannel with Vortex-Generators, Proceedings of AIAA-2006, AIAA/ASME Joint Thermophysics and Heat Transfer Conference, 2006, San Francisco, CA.

5. REFERENCES

[1]. Tuckerman, D. B., and Pease, R. F., High-performance heat sinking for VLSL, IEEE Electron Device Letters, vol. EDL-2, pp. 126-129, 1981.

[2]. Fiebig, M., Vortex generators for compact heat exchangers, Journal of Enhanced Heat Transfer, vol. 2, pp. 43-61, 1995.

[3]. Fiebig, M., Embedded vortices in internal flow: heat transfer and pressure loss enhancement, *International Journal of Heat and Fluid Flow*, vol. 16, pp. 376-388, 1995.

[4]. Maurel, A., Ern, P., Zielinska, B. J. A., and Wesfreid, J. E., Experimetnal study of self-sustained oscillations in a confined jet, *Physical Review E*, vol. 54, pp.3643-3651, 1996.

[5]. Saha, A. K, and Acharya, S., Three-dimensional flow and heat transfer calculations in micro-channel heat exchangers, *ASME International Mechanical Engineering Congress and Exposition*, New York, New York, Nov. 11-16, 2001.

[6]. Wu, P. Y., Little, W. A., Measurement of the heat transfer characteristics of gas flow in fine channel heat exchanger used for microminiature refrigerators, *Cryogenics*, vol. 24, pp. 415-420, 1984.

[7]. Choi, S. B., Barron, R. F., Warrington, R. O., Fluid flow and heat transfer in microtubes, *Micromechanical Sensors, Actuators and Systems*, Atlanta, GA, pp. 123-134, 1991.

[8]. Peng, X. F., Peterson, G. P., Wang, B. X., Heat transfer characteristics of water flowing through micro channels, *Experimental Heat Transfer*, vol. 7, pp. 265-283. 1994.

[9]. Mo, H. L., Characteristics of friction factor of gas flowing through small rectangular ducts, *Cryogenics*, vol. 38, pp. 869-873, 1998.

[10]. Mala, G. M., Li, D. Q., and Dale, J. D., Heat transfer and fluid flow in microchannels, *International Journal of Heat and Mass Transfer*, vol. 40, pp. 3079-3088, 1997.

[11]. Adams, T. M., Ghiaasiaan, S. M., and Abdel-Khalik, S. I., Enhancement of liquid forced convection heat transfer in microchannels due to the release of dissolved noncondensables, *International Journal of Heat and Mass Transfer*, vol. 42, pp. 3563-3573, 1999.

[12]. Saha, A. K., Muralidhar, K., and Biswas, G., Transition and chaos in two-dimensional flow past a square cylinder, *Journal of Engineering Mechanics*, pp. 523-532, May 2000.

[13]. Saha, A. K., Biswas, G., and Muralidhar, K., Three-dimensional study of flow past a square cylinder at low Reynolds number, *International Journal of Heat and Fluid Flow*, vol. 24, pp. 54-66, 2003.

[14]. Saha, A. K, and Acharya, S., Effect of cylinder aspect ratio and channel dimensions on the fluid flow and heat transfer in parallel-plate channel heat exchangers, *ASME International Mechanical Engineering Congress and Exposition*, New Orleans, Louisiana, Nov. 17-22, 2002.

[15]. Valencia, A., Heat transfer enhancement due to self-sustained oscillating transverse vortices in channels with periodically mounted rectangular bars, *International Journal of Heat and Mass Transfer*, vol. 42, pp. 2053-2062, 1999.

[16]. Valencia, A., Heat transfer enhancement in a channel with a built-in square cylinder, *International Communications in Heat and Mass Transfer*, vol. 22, pp. 47-58, 1995.

[17]. Valencia, A., Turbulent flow and heat transfer in a channel with a square bar detached from the wall, *Numerical Heat Transfer*, Part A, vol. 37, pp. 289-306, 2000.

[18]. Grosse-Gorgemann, A., Weber, D., and Fiebig, M., Experimental and numerical investigation of self-sustained oscillations in channels with periodic structures, *Experimental Thermal and Fluid Science*, vol. 11, pp. 226-233, 1995.

[19]. Zhang, L. W., Tafti, D. K., Najjar, F. M., and Balachandar, S., Computations of flow and heat transfer in parallel-plate fin heat exchangers on the CM-5: effects of flow unsteadiness and three-dimensionality,

International Journal of Heat and Mass Transfer, vol. 40, pp. 1325-1341, 1997.

[20]. Zhang, L. W., Balachandar, S., Tafti, D. K., and Najjar, F. M., Heat transfer enhancement mechanisms in inline and staggered parallel-plate fin heat exchangers, *International Journal of Heat and Mass Transfer*, vol. 40, pp. 2307-2325, 1997.

[21]. Amon, C. H. and Mikic, B. B., Spectral element simulations of unsteady forced convective heat transfer: Application to compact heat exchanger geometries, *Numerical Heat Transfer*, Part A, vol. 19, pp. 1-19, 1991.

[22]. Amon, C. H., Majumdar, D., Herman, C. V., Mayinger, F., Mikic, B. B. and Sekulic, D. P., Numerical and experimental studies of self-sustained oscillatory flows in communicating channels, *International Journal of Heat and Mass Transfer*, vol. 35, pp. 3115-3129, 1992.

[23]. Bosch, G. and Rodi, W., Simulation of vortex shedding past a square cylinder with different turbulence models, *International Journal for Numerical Methods in Fluids*, vol. 28, pp. 601-616, 1998.

[24]. Hsieh, S. S., Lin, C. Y., Huang, C. F. and Tsai, H.H., Liquid flow in a micro-channel, *Journal of micromechanics and microengineering*, vol. 14, pp. 436-445, 2004.

[25]. Judy, J., Maynes, D. and Webb, B. W., Characterization of frictional pressure drop for liquid flows through microchannels, *International Journal of Heat and Mass Transfer*, vol. 45, pp. 3477-3489, 2002.

[26]. Wu, H. Y. and Cheng, P., Friction factors in smooth trapezoidal silicon microchannels with different aspect ratios, *International Journal of Heat and Mass Transfer*, vol. 46, pp. 2519-2525, 2003.

[27]. Qu, W. L., Mala, G. M., and Li, D. Q., Pressure-driven water flows in trapezoidal silicon microchannels, International Journal of Heat and Mass Transfer, vol. 43, pp. 353-364, 2000.

[28]. Wang, B. X., Peng, X. F., Experimental investigation on forced convection heat transfer through microchannels, International Journal of Heat Mass Transfer, 37 (1), pp. 73-82, 1994.

[29]. Poh-Seng Lee, Suresh V. Garimella and Dong Liu, Investigation of heat transfer in rectangular microchannels, International Journal of Heat and Mass Transfer, 48, 1688-1704, 2005.

[30]. Weilin Qu, Issam Mudawar, Experimental and numerical study of pressure drop and heat transfer in a single-phase micro-channel heat sink, International Journal of Heat and Mass Transfer, 45, 2549–2565, 2002

[31]. Peng, X. F. and Peterson, G. P., Convective heat transfer and flow friction for water flow in microchannel structure, International journal of heat and mass transfer, vol. 39, pp. 2599-5608, 1996.

[32]. Braza, M., Chassaing, P., and Minh, H.H., Numerical Study and Physical Analysis of the Pressure and Velocity Fields in the Near Wake of a Circular Cylinder, J. Fluid Mech., 165, 79-130, 1986.